AD-A260 474

CUMENTATION PAGE

Form Approved
OMB No. 0704-0188

(2)

2. REPORT DATE	3. REPORT TYPE AND DATES COVERED
Oct. 20, 1992	Final Report, Mar.1 to Sep.1 '92

4. TITLE AND SUBTITLE
Final Report for "Novel Optical Processor for Phased Array Antenna."

5. FUNDING NUMBERS
DAAL03-92-C-0009

6. AUTHOR(S)
Dr. Shi-Kay Yao

7. PERFORMING ORGANIZATION NAME(S) AND ADDRESS(ES)
Optech Laboratory
1560 Brookhollow Drive #113
Santa Ana, CA 92705

93-03131
54pp

9. SPONSORING/MONITORING AGENCY NAME(S) AND ADDRESS(ES)
U. S. Army Research Office
P. O. Box 12211
Research Triangle Park, NC 27709-2211

10. SPONSORING/MONITORING AGENCY REPORT NUMBER
ARO 29477.1-EL-SBI

11. SUPPLEMENTARY NOTES
The view, opinions and/or findings contained in this report are those of the author(s) and should not be construed as an official Department of the Army position, policy, or decision, unless so designated by other documentation.

12a. DISTRIBUTION/AVAILABILITY STATEMENT
Approved for public release; distribution unlimited.

12b. DISTRIBUTION CODE

13. ABSTRACT *(Maximum 200 words)*

Investigations are conducted on two novel optical devices, namely a fiber-optic phase conjugation loop for cancellation of phase jitter noise in RF distribution network and an acousto-optic imaging spatial light modulator. Analytical as well as experimental studies have been performed on several critical technical issues with success. Developmental issues and phase II program have been outlined for further development towards experimental demonstration of the proposed technologies and systems.

14. SUBJECT TERMS
Phase Conjugation, Spatial Light Modulator, RF Distribution, Phased Array Antenna.

15. NUMBER OF PAGES
53

16. PRICE CODE

17. SECURITY CLASSIFICATION OF REPORT	18. SECURITY CLASSIFICATION OF THIS PAGE	19. SECURITY CLASSIFICATION OF ABSTRACT	20. LIMITATION OF ABSTRACT
UNCLASSIFIED	UNCLASSIFIED	UNCLASSIFIED	UL

FINAL TECHNICAL REPORT
Item Number Supplies/Services: CLIN 0002 AB

For: NOVEL OPTICAL PROCESSOR FOR PHASED ARRAY ANTENNA

Contract Number: DAAL03-92-C-0009

Issued by: U.S. ARMY RESEARCH OFFICE
P.O. Box 12211
Research Triangle Park, NC 27709-2211

Attn: Patsy S. Ashe

Covering: Mar. 1 to Aug. 31, 1992

Deliver to: U.S. ARMY RESEARCH OFFICE
Attn: Richard O. Ulsh
P.O. Box 12211
Research Triangle Park, NC 27709-2211

Prepared by: OPTECH LABORATORY, Code OLBH8
1560 Brookhollow Drive #113
Santa Ana, California 92705

Preparation Date: Dec. 15, 1992

--- Unclassified ---

TABLE OF CONTENTS:

FINAL TECHNICAL REPORT for
NOVEL OPTICAL PROCESSOR FOR PHASED ARRAY ANTENNA (DAAL03-92-C-0009)

1.0 ABSTRACT:

Preliminary investigations are conducted on two novel optical devices, namely a fiber-optical phase conjugation loop and an imaging acousto-optic spatial light modulator, for the purpose of optical signal processor development for phased array antenna applications. The fiber optical phase conjugatin loop can be useful for the cancellation of phase jitter noise in RF reference waveforms transmitted through optical fibers. The imaging acousto-optic spatial light modulator has the potential of becoming an extremely high speed spatial light modulator for wideband microwave signal processing applications.

The investigations lead to experimental demonstration of the feasibility and the fundamental properties of these proposed devices. Analytical study has been carried out for determining the ultimate usefulness of these devices.

Developmental issues and phase II advanced developments has been outlined for further development of the novel optical processors based on these new devices.

2.0 INTRODUCTION AND BACKGROUND:

Beam forming signal processing and signal distribution are major issues for large microwave phased array. Extremely tight tolerances and stability requirement of the microwave distribution network and real time multiple beam forming with interference cancellation are nearly unsurmountable problems for conventional approaches. In addition, size, weight, and cost reduction for large phased array system is crucial for many potential applications that require mobility.

In an active phased array, RF generation and distribution can be provided by stabilized laser diodes and optical fiber networks[1-3] with advantages of low loss, low dispersion, high bandwidth, low cross-coupling, and low cost. Generation of true time delay and/or phase tap weights can be done by optical switching network or Fourier optical processor. Many of the basic technology concepts such as RF generation using injection laser diodes, microwave optical link, opto-microwave interaction, optical generation of true time delay, fourier optical beam forming processor, and optical correlation interference cancellation loops have been demonstrated during the past ten years[4-11]. Optical technologies may provide the solutions for the near future[12].

Although fiber optical RF link is reasonably mature technology, the very tight delay jitter requirement among signals transmitted through a group of fibers is a challenging problem limiting high frequency applications. Another major issue is in real time beam forming processing for weight generation or signal delay setting. Computing the antenna weights for steering of one or more antenna beams to predetermined locations can be done digitally without too much difficulty. However, in the dynamic environment of tracking several uncooperative objects with adaptive interference cancellation, one needs to conduct computational intensive operations such as fourier transform, matrix inversion,

or multi-channel signal correlation in real time. Many acousto-optic processor architectures have been proposed for real time beam forming applications[13,14]. Fourier transform processors were investigated for beam steering weight generation. Acousto-optic correlation interference cancellation loop processors[8,13-18] based on Applebaum's model have been demonstrated for null steering, but appears rather complicated. Although the feasibility of acousto-optic signal processing technology for beam forming applications appears promising, using two different acousto-optical processors for similar functions seems leaving much room for further advancement of the acousto-optics processor technology.

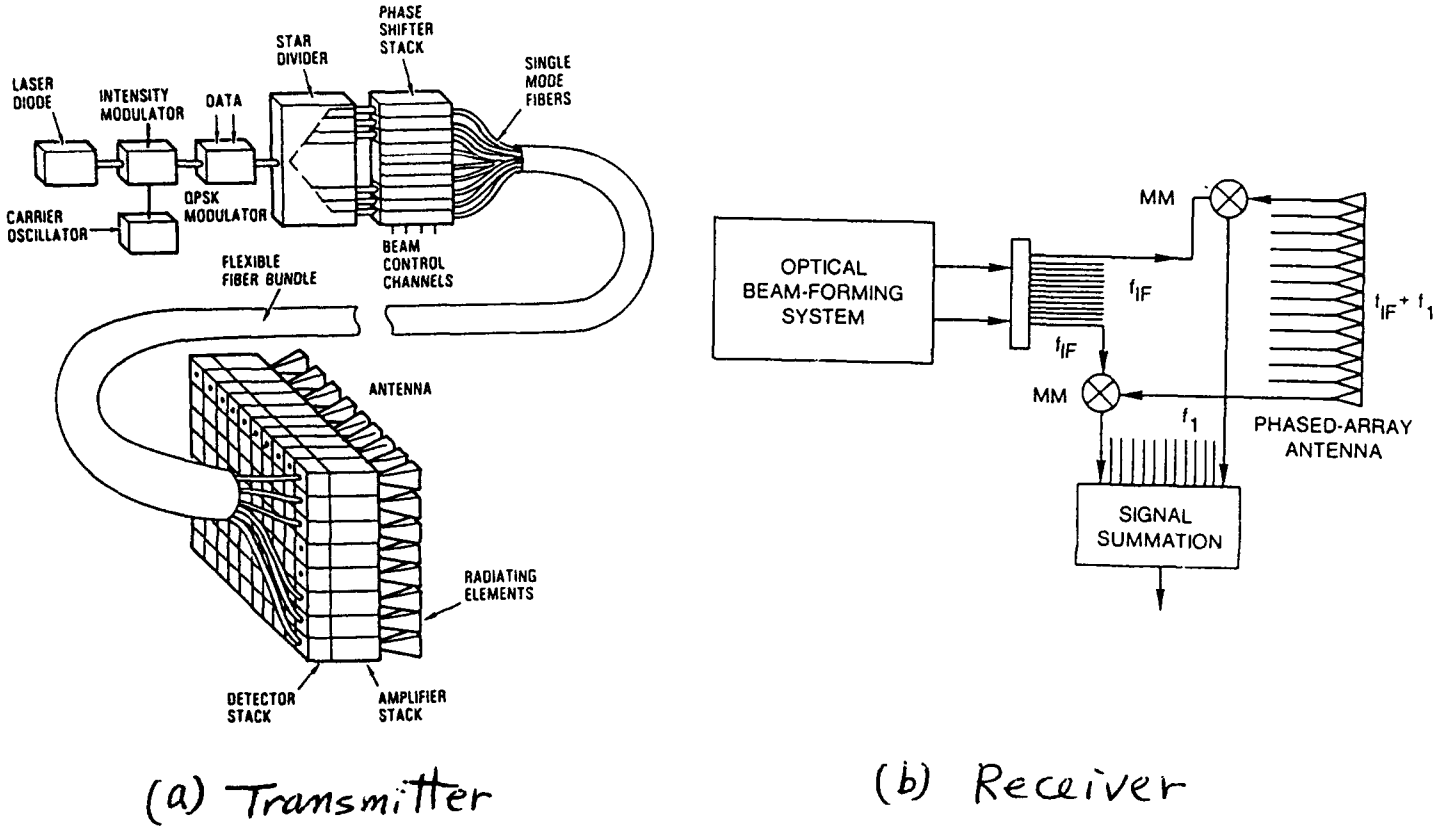

FIGURE 1, Conceptual System of Fiber Optical Phased Array Antenna.

Current status of optical technologies may be close to eventual demonstration of a low frequency (up to 2 GHz) medium sized antenna array (10 by 10). For higher frequency and larger arrays, opportunities for technology improvements include (a) transmission of optical carrier or high frequency RF carrier through a group of long fibers without excessive differential phase jitter, (b) more advanced beam forming processor for adaptive steering of main antenna beams and nulls, and (c) improved performance in opto-microwave interaction devices. This proposed SBIR program addresses the first two issues with new and novel device and subsystem concepts. Phase conjugation using photorefractive process is proposed for jitter free delivery of RF through a group of optical fibers. Unified acousto-optic processor for both beam and null steering and perhaps even as a phased array receiver will be studied using a new concept of acousto-optic imaging 2-D wideband SLM.

The proposed technology developments promote the general concept of separating RF carrier delivery from data and weight delivery, and coherent real time fourier transform processor receiver. There will be two optical subsystems, one jitter free fiber network for RF carrier distribution, and one acousto-optic real time fourier transform imaging receiver/ beam former. The beam forming processor output is an array of data streams each contains data and weight riding on an IF which, due to relatively low frequency, is insensitive to small delay jitter in fibers. The potential value of the fourier processor for null steering on the active array will be studied.

Other than the need to develop a phase conjugation jitter servo fiber network, a wideband spatial light modulator array capable of refreshing the image at nano-seconds frame rate is highly desirable. Among the spatial light modulator technologies to date, only acousto-optic spatial light modulator can provide such modulation bandwidth. For real time processing of 2-D phased array antenna signal, a wideband 2-D spatial light modulator array must be developed.

3.0 PROPOSED OPTICAL PROCESSORS FOR PHASED ARRAY ANTENNA:

The overall technical objective of this program is to develop a practical optical signal processor and a fiber optic signal distribution means for weight, size, and cost reduction of future phased array antennas and for providing technological thrust for more capable phased array systems operating at higher frequencies. Major technical issues in both optical fiber delay jitter and optic beam forming processors will be tackled with new and novel device concepts. The phase I SBIR program is to establish the feasibility and potential performances of a novel RF distribution network using phase conjugation in photo-refractive medium, and the feasibility of an acousto-optic processor for both beam and null steering using a new 2-D wideband SLM based on acousto-optic imaging.

The specific technical questions that will be answered during the proposed phase I program are (1) will the phase conjugation optical fiber network perform for jitter free RF distribution, (2) are the photorefractive materials available to date good enough for such applications, (3) how to construct and what are performance limitations of the imaging acousto-optic 2-D wideband spatial light modulator, (4) is it possible to use a fourier optical processor for phased array interference cancellation, and (5) how will these new technologies impact future development of optical controlled phased array systems.

The phase I program is organized into four (4) major tasks listed as follows.

Task 1. Jitter Free RF Distribution Feasibility: Feasibility of jitter free RF distribution using phase conjugation and or other methods will be studied analytically. Simplified experiments demonstrating phase jitter compensation will be conducted. Results will be interpreted for phased array antenna applications.

Task 2. Wideband 2-D SLM Feasibility Analysis: Feasibility of wideband 2-D spatial light modulator, properties, and limitations will be analyzed. Acousto-optic imaging experiments will be conducted to verify key parameters. Potential application for phased array antenna beam forming processor will be accessed.

Task 3. Beam Forming Processor Analysis: Potential applications of the fourier transform beam forming processor with or without the wideband 2-D spatial light modulator will be analyzed. Expansion of such processor architecture for adaptive interference cancellation (null steering) will be investigated.

Task 4. Technical Reports: Monthly technical reports will be prepared. Final technical report summarizing all investigation findings and recommended phase II developments will be presented at the end of project.

4.0 FIBER-OPTIC RF DISTRIBUTION LINKS:

Fiber optics RF distribution network can greatly reduce the size, weight, and cost of the feed manifold. Fiber optic RF links with up to 20 GHz of bandwidth has been developed. Wideband signal may be transmitted either incoherently (optical) or coherently. Phase and amplitude weights and delay commands are easily distributed by fiber optics network due to relatively low data rates. Time delay generation can also be achieved using established fiber optical switch array technology on delay line branches.

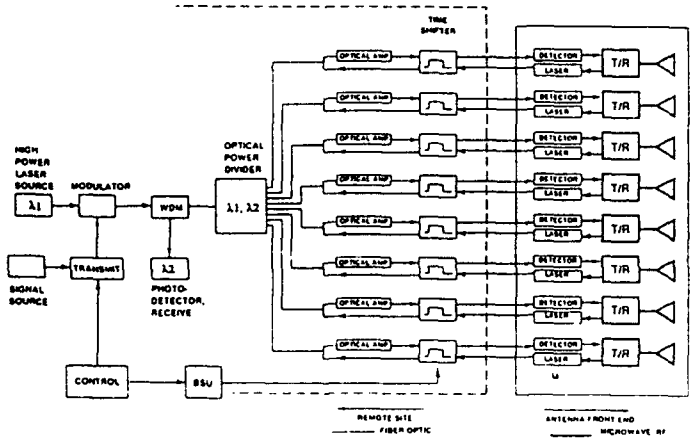

Architecture of a Photonic Phased Array

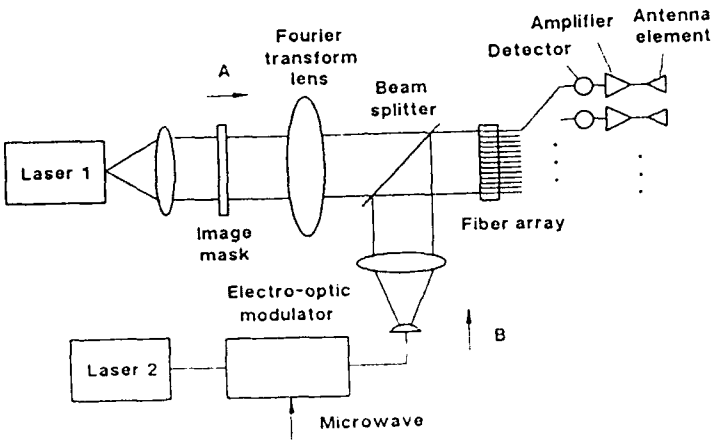

Fourier optic processor for phased array

Figure 2, Several Proposed Fiber Optical Distribution Systems Of Phased Array Signal.

However, due to temperature and stress induced differential delay jitter among long optical fibers, relative phase coherence of a group of light beams transmitting through

different fibers is difficult to maintain. Therefore, RF signal are transmitted as intensity modulation envelope on optical carrier. Comparing to amplitude or phase modulation, intensity modulation is less sensitive to optical phase jitter by five orders of magnitude due to the much longer microwave wavelength comparing to optical wavelength. Figure 2 illustrates several proposed schemes for RF distribution by optical fibers.

4.1 TECHNICAL ISSUES:

Optical fibers exhibit less thermal expansion than metallic waveguides with its delay temperature coefficient in the order of a few ppm. However, phase jitter is inversely proportional to wavelength. Due to the small wavelength of light, optical fiber segments are often made into temperature or pressure sensors. Optical phase shift of 180 degree can be the result of only 2×10^{-9} length variation for a 100 meter length of fiber.

Transmission of RF waveform as intensity modulation envelope on optical carrier is insensitive of optical carrier phase jitter. However, a delay drift of 1 ps (corresponding to thermal expansion of about a hundred micron, about 1×10^{-6} of a 100 m fiber) can still cause 3.6 degree of phase error in a 10 GHz waveform. Whether we chose to transmit the RF carrier only or the processed modulated RF signal to individual array elements, the delay jitter is a problem limiting the performances of fiber optical phased array antenna. Even in a system that only send the weight and delay commands as well as channel data by optical fibers, we still have to come up with a means to synchronize the distributed local RF sources at each array element to a master oscillator. This delay drift among optical fibers must be overcome by either improved fiber construction or by novel optical signal processing techniques for optical phased array antenna technology to be useful in large phased arrays at higher frequency ranges.

4.2 PHASE JITTER DETECTION USING PHASE CONJUGATION MIRROR:

The phase jitter in a transmission line can be neutralized if the amount of phase jitter can be measured at the receiving end of the transmission line. Unfortunately, this is a rather difficult problem.

Recent advances in optical phase conjugation signal processing provide an exotic solution to the problem of phase jitter measurement at the receiving end of a transmission line. Figure 3 illustrates the unique properties of optical phase conjugation mirror, in free space and through a piece of optical fiber. Figure 3 c) illustrates the use of optical phase conjugation mirror for the measurement of unknown phase variation at the receiving end of an optical fiber. Since the phase conjugate reflection beam follows as retro-reflective path, it will be self aligned for coupling into the optical fiber.

In figure 3, the key element is the photorefractive nonlinear crystal in-which the reflection with conjugate phase is generated. Recent advances in phase conjugation technology have improved the photorefractive nonlinear crystal in both sensitivity, efficiency and response time. Using some of the newer materials such as BaTiO3 or KNSBN, efficiency as high as 60% can be achieved, making such process practical for potential applications.

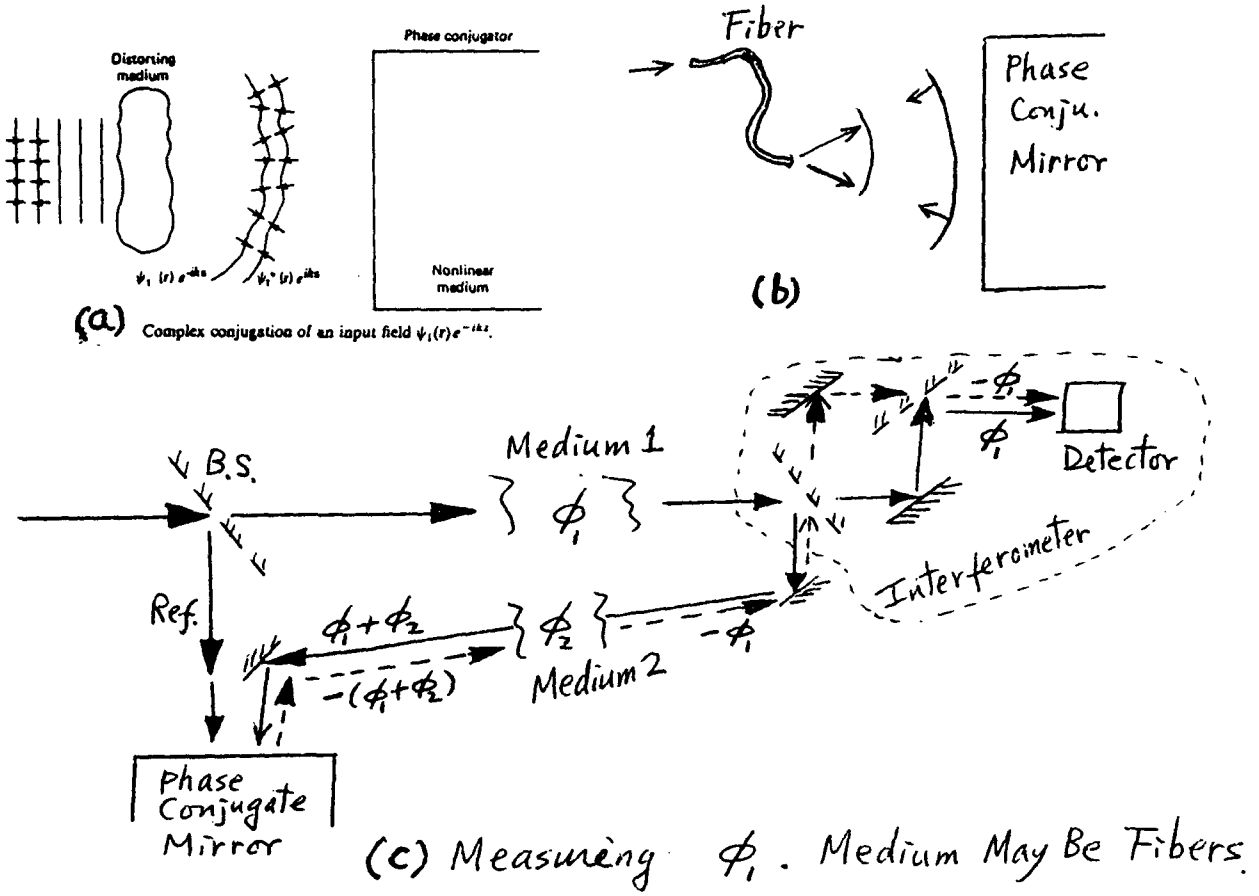

Figure 3, Optical Phase Conjugation Mirror in a) Free Space, b) Through the Fiber Transmission, and c) A Set-up for Phase Jitter Measurement.

4.3 ELIMINATION OF PHASE JITTER NOISE:

If the phase drift is slow comparing to the rise time of a photorefractive material, phase conjugation technique may be applied to neutralize random phase drift in optical systems. For the present application, the conjugate reflection of a laser beam from a single mode optical fiber is a retro-reflected laser beam carrying a negative value of phase. Note that the term "negative phase" is referenced to the phase of reference wavefronts such as the pump beam.

The proposed scheme for elimination of phase jitter in fiber optical transmission is illustrated by figure 4. A portion of the master laser beam is sent through a fiber making a loop around an phased array element and back to the master laser site. The light output after going through the fiber loop assumes a net phase difference of $\phi1+\phi2+\phi3$ comparing to reference light from the master laser. Note $\phi1$, $\phi2$, and $\phi3$ denotes net phase shifts in the section of fiber from master laser to array element, in the optical circuit at the array element, and in the section of fiber from the array element back to the master laser respectively. At the array element end of the fiber loop, a four wave mixing phase conjugation device is set-up in a photorefractive crystal using the fiber output and master laser beams with the master laser as pump beam. Erbium doped fiber amplifiers may be used if laser beam intensity falls below threshold required to achieve certain phase

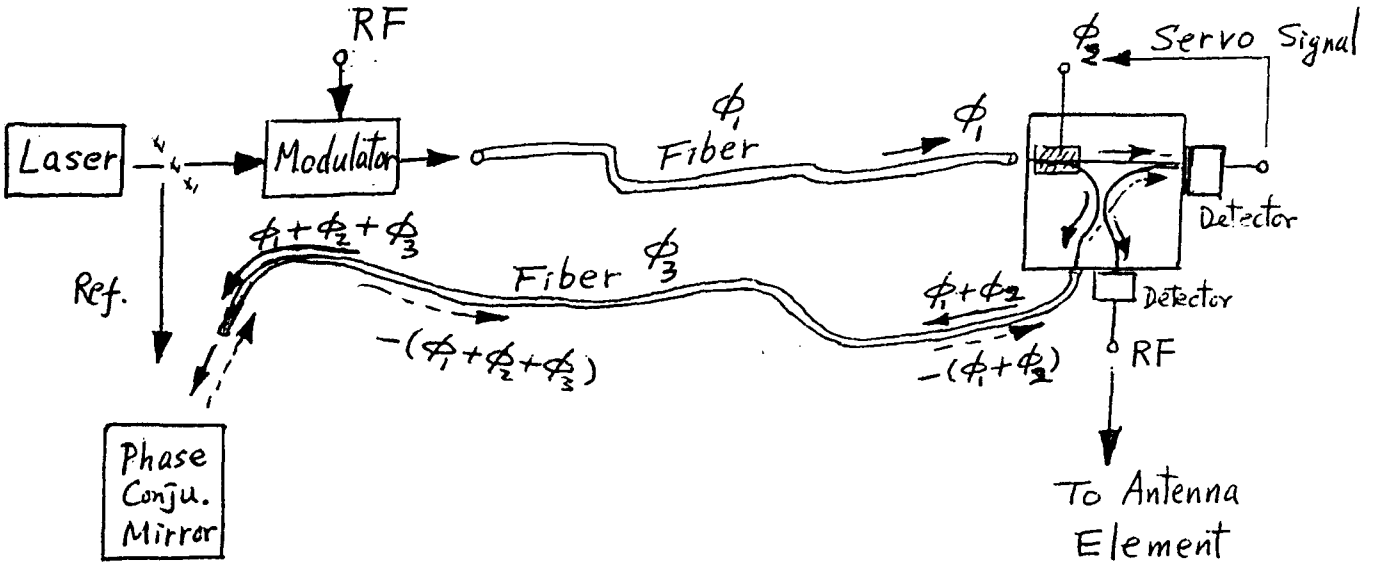

Figure 4, Phase Conjugate Fiber Loop Concept for Jitter Free RF Distribution.

conjugation rise time. An amplified phased conjugated beam shall be produced back tracing through the fiber loop towards the master laser. The phase conjugated return beam shall exhibit a net phase of $-(\phi1+\phi2+\phi3)+\phi3=-(\phi1+\phi2)$ at the array element end of the fiber loop. Using fiber or integrated optical couplers, we will be able to compare the phase in forward and backward light at array element and they are $(\phi1+\phi2)$ for the forward light and $-(\phi1+\phi2)$ for the backward light. Our philosophy is to adjust $\phi2$ to $-\phi1$ and that will make the two phase values equal and interfere constructively. The constructive interference is used to servo $\phi2$. Thus, the light phase at this array element shall become in phase with the master laser with fiber fluctuation $\phi1$ neutralized.

Although the 2π degeneracy of an optical interferometer causes multiple solutions of $\phi2$ separated by 2π, the system will be stabilized with respect to delay jitter in the fiber. Also, note that the specific point chosen as array element is somewhat arbitrary from microscopic point of view. Since part of the optical waveguide branches off the main fiber loop and is therefore not in the phase conjugation path, residual phase error may occur. As long as the branch-off is balanced and short, and the integrated optics chip has uniform temperature and low thermal coefficients, the variable part of the residual error will be many orders smaller than the variable drift due to fiber which is now neutralized. As the fiber drifts, the phase conjugator will follow, and the phase shifter $\phi2$ will be servoed to follow fiber drift by keeping the interference constructive. Phase stabilized RF signal will be available after the servo.

4.4 CHARACTERIZATION OF PHASE CONJUGATION MIRROR:

The critical technology in the proposed scheme of figure 4 is the phase conjugation reflector mirror. During the last ten years, the physics of phase conjugation[19,20] and its potential applications have been the focus of intensive scientific investigations. The nonlinear optical phenomena is based on optical diffraction from a real time photorefractive grating written inside an electro-optic medium by the intersecting laser beams, one signal beam and one intense pump beam. The phase conjugation output beam arises from reading the grating by another intense laser beam. Since the output beam intensity is proportional to the intensity of the read beam, optical amplification gain is possible when the pump beams are much stronger than the signal beam.

In order to obtain reasonable output efficiency and response time, high intensity laser beams are generally required. Recent advances in nonlinear optical materials has been able to reduce the power requirement dramatically and efficiency as high as 60% has been reported with pump beams of only about 10 milli-watts. In the mean time, response time as short as micro-seconds has been reported using certain semiconductive materials near its band-edge.

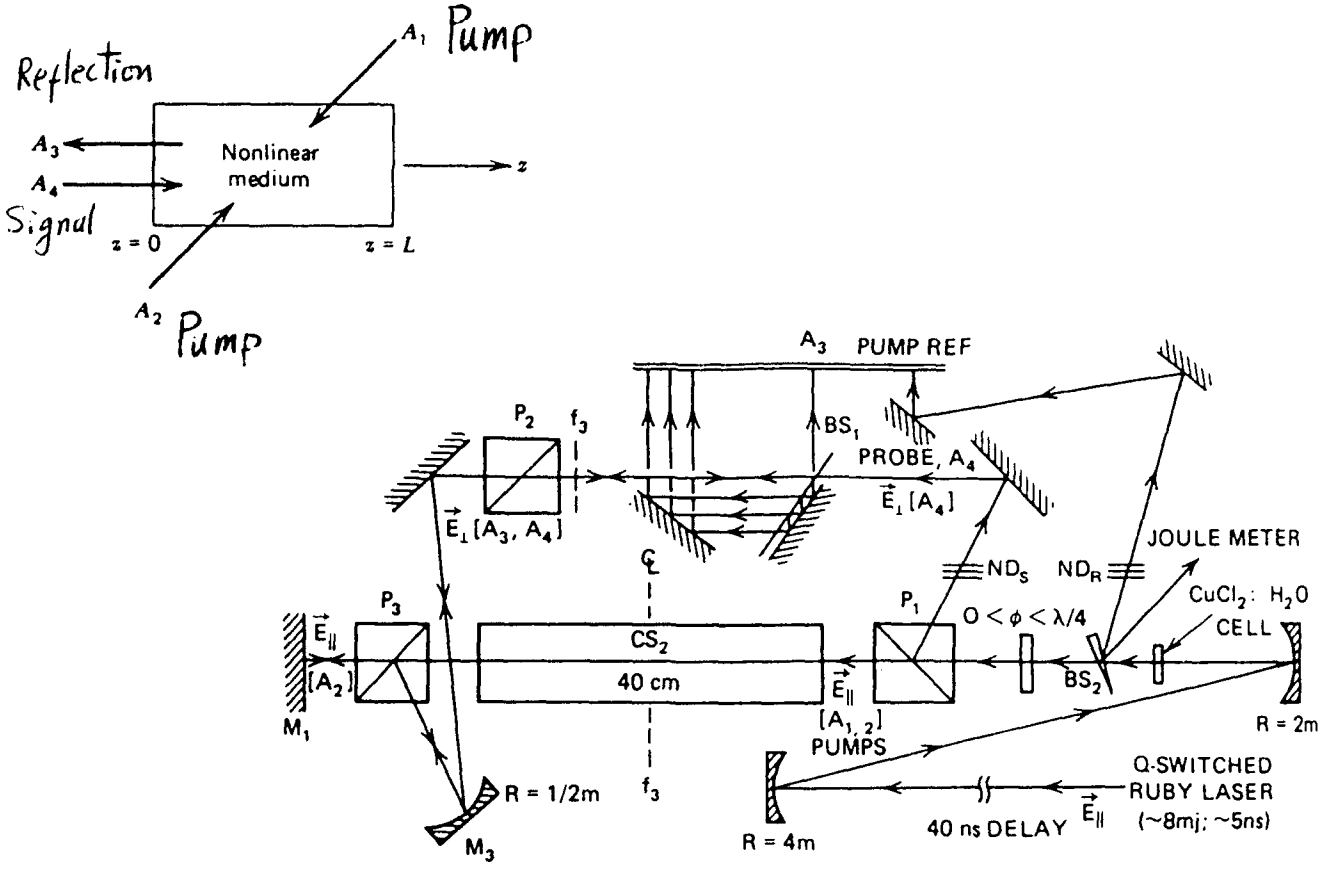

Experimental apparatus for measurement of the nonlinear reflection coefficient (all mirrors are totally reflecting).

Figure 5, Four Wave Mixing Phase Conjugation Mirror Configurations.

4.4.1 CHOICE OF PHASE CONJUGATION CONFIGURATIONS:

Several optical configurations have been reported including four-wave-mixing and self-pumped-phase-conjugation-mirror. The optical configuration of four-wave-mixing is highly useful in studying the physics behind the phenomena, and is known to be capable of providing gain to a weak signal beam. On the other hand, the self-pumped-phase-conjugation-mirror (SPPC Mirror) is easier to operate since most of the optical alignment requirements are provided by careful orientation and shapping of the nonlinear optical crystal in the form of a nonlinear optical device.

For the intended application, it is necessary to generate a phase conjugate reflection from the optical output after transmission through an optical fiber, which sometimes may be rather weak. The four-wave-mixing configuration is interesting due to its optical gain, but is too complicated for future field applications. The SPPC mirror configuration is very interesting due to its simple device configuration and reported high efficiency approaching 60% reflectivity. However, it requires hundreds of milliwatt of laser intensity in order to exhibit fast response time shorter than a few seconds. Based on the CAT arrangement of SPPC mirror, a KITTY[21] arrangement has been reported that is capable of providing phase conjugate reflection of a weak beam with fast response time. It was reported that the response time of a KITTY mirror is dictated by the SPPC mirror efficiency and response time of the much stronger pump beams. Such arrangement will be more suited for the intended application of this program.

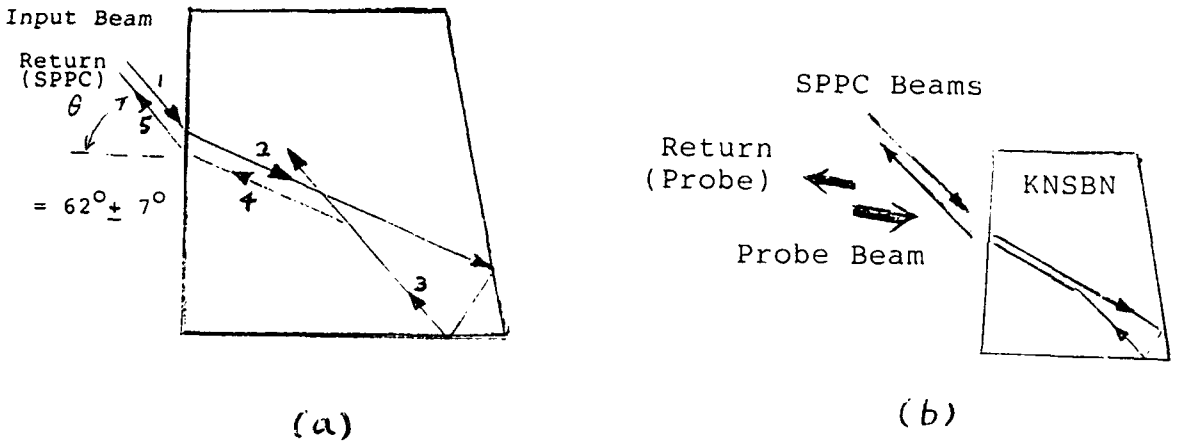

(a) The KNSBN SPPC Crystal. Input Beam at 62° has angular Range of ± 7°. Input, 1, goes into crystal, ray 2, reflects as ray 3 which crosses ray 2. The Phase Conjugation Grating in the cross region generates the SPPC return beam as ray 4 and ray 5.

(b) Use of The SPPC Crystal in the "Kitty" Arrangement. The Probe Beam is the Information Carrying Beam. The Probe Beam Must Stay Within The ± 7° Angle of Acceptance of the SPPC Beam. Even When the probe Beam May Be Much Weaker Than The SPPC Beam, The Phase Conjugate Mirror Response Time for The Probe Beam Will Be Dictated By The SPPC Beam.

Figure 6, The SPPC Mirror and The KITTY Phase Conjugate Mirror.

4.4.2 CHOICE OF MATERIAL:

In order to improve efficiency, materials with large electro-optic coefficients and high photo-carrier and trap density are preferred. Recent advances in nonlinear optical materials has been able to reduce the power requirement dramatically and efficiency as high as 60% has been reported with pump beams of about 10 milli-watts using Fe doped LiNbO3, Potasium Niobate, BaTiO3, SBN and KN:SBN[22] of various doping materials. Other materials of interest includes semiconductive materials with exiton absorption and quantum well materials. The dielectric materials have higher electo-optic coefficients and can lead to higher diffraction efficiency.

In order for the photorefractive material to function, some optical absorption with photoconductivity is necessary. The absorbed photon generates photoconductive carriers which forms the photorefractive gratings when trapped in a light intensity related pattern. The absorption bands of the dielectric materials are in the visible wavelengths with best efficiency in the blue green part of the sepctrum. Proper doping can tailor the absorption band and efficiency of the dielectric materials for improved performances for given application. Popular doping materials for KNSBN includes Co, Cu, Ce, Fe, and Cr. The semiconductive materials has a smaller bandgap than the dielectric materials and its best efficiency are in the red to near infrared spectrum.

The response time is mostly function of photo-conductivity, carrier mobility and the applied drift field. It is also a function of pump beam laser intensity which provides the photo-carriers for forming the photorefractive gratings. For dielectric photorefractive materials, the response time is in the order of milli-seconds to many seconds. On the other hand, response time in the micro-seconds has been observed in semiconductive photorefractive materials such as GaP and InP.

For the intended applications, use of semiconductive photorefractive material shall be recommended due to the injection laser diode competible operation wavelength and the fast response time. However, for the feasibility study, dielectric photorefractive materials can be useful due to higher demonstrated phase conjugation reflection efficiency at relatively low laser intensity levels. Another advantage of using the dielectric materials for the phase I experiments is the availability of well developed high power Ar ion lasers. KNSBN crystal is selected because of the highest reported phase conjugation reflectivity comparable to BaTiO3, better material uniformity, and ease of handling without concern of phase transition due to ambient temperature.

Several major potential issues exist in view of intended future applications in a fiber optical system. These are (1) the need of blue-green optical wavelength for efficient phase conjugation operations, (2) the relatively slow response time with a few milliwatts of laser unless a high intensity laser beam is employed, and (3) the coherence required between the laser beams engaged. These issues may be resolved by using semi-conductive photorefractive materials such as GaAs, GaP, and InP for phase conjugation mirror in conjunction with stabilized high power laser diodes. These materials have reported response times in the order of micro-second at laser diode wavelengths.

For instance, R. Montgomery et.al.[23] has demonstrated an adaptive canceler loop using injection laser diodes of 1.2 and 1.3 micron wavelengths and indium phosphate photorefractive devices with time constants in the micro-seconds to milliseconds range. In the mean time, diode lasers at 0.81 micron wavelength with 0.2 watt and 1 watt output power are now available from Spectra-Diode.

Long coherence length laser radiation can be available utilizing stabilized cw single transverse mode laser diodes. Since most cw single mode laser diodes tend to exhibit single longitudinal mode behavior when operated significantly above laser threshold, instantaneous laser line width is usually in the order of KHz to MHz. Using a combination of temperature control servo and a drive current servo, stabilized laser diode line-width as narrow as a few KHz has been demonstrated in the eighties. The coherent length required for a fiber system with 200 meters of fiber length is about 1 MHz which is well within the limit of previously demonstrated capabilities.

4.4.3 CHARACTERIZING THE SPPC DEVICE:

Figure 7 illustrates the shape of the KNSBN photorefractive crystal used as a SPPC device. When an Ar ion laser beam at 488nm or 514.5 nm wavelength enters the crystal from one side as illustrated, it goes through a corner reflection at the lower right hand corner. Since this corner is made less than 90 degree, the reflection will be tilted away from the incident beam direction as shown. Note the overlap region for the forward and the reflected beams inside the crystal within which phase conjugation mechanism is expected to take place. The schematic of the preliminary experimental set-up for evaluation of this SPPC crystal is given by figure 8. A beam splitter is used for monitoring the self-pump phase conjugate mirror output which is expected to follow a retro-reflection path back towards the laser.

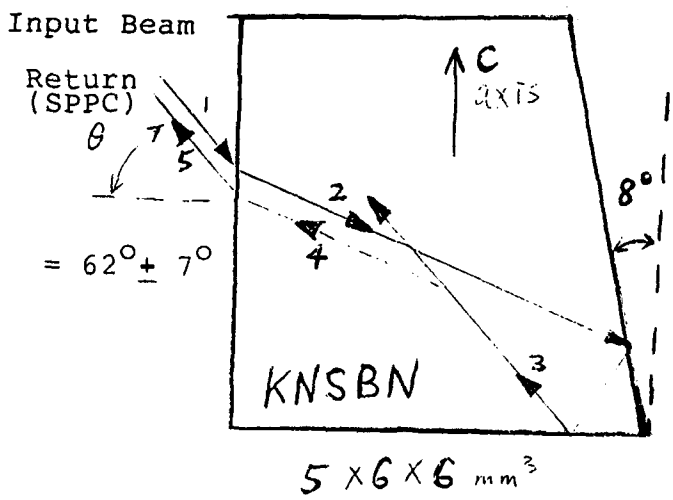

Figure 7, Shape of the SPPC Mirror Crystal made of KNSBN.

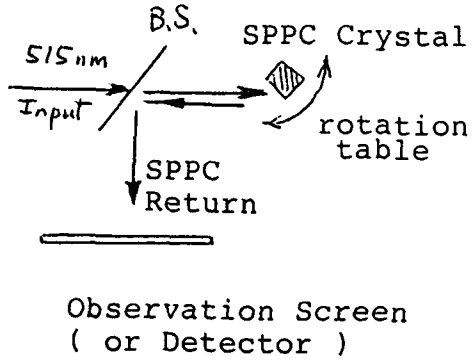

Figure 8, Preliminary Experimental Set-Up for Evaluation of the SPPC Device.

According to the crystal grower, with adequate laser power this crystal shall be capable of SPPC activity with the following parameters

SPPC reflectivity	up to 30%
Threshold Power	0.02 W/cm^2
Response Time (e^{-1})	20 sec.

When a 488nm laser beam is directed into the KNSBN SPPC crystal, a very faint SPPC mirror reflection is observed after about one second. The spot intensity grows steadily and reaches a level of about 25% in approximately 1 minute. The laser power used is about 15 milli-watt with a beam diameter of about 2mm. At a lower laser beam power of 5 mw, the reflection reaches 22% in about 5 minutes.

After the initial experiment, the optical incidence angle to the KNSBN crystal is rotated for examining the acceptance angle of the SPPC mirror. By starting from normal incidence, SPPC action was observed for the angular range of 55 to 69 degrees. Thus, an acceptance angle range of 14 degree is available for information carrying optical wavefronts.

The proposed "KITTY" configuration[21] is illustrated by figure 6. At first, a stronger local oscillator beam will be used to establish the SPPC activity in the KNSBN crystal. Subsequently, a signal beam is introduced to the crystal and a phase conjugation return beam shall be expected with the time constant dominated by the SPPC response time of the stronger local oscillator beam. Because the KITTY performances are dictated by the SPPC mirror performances, careful characterization of the SPPC mirror performances of the KNSBN crystal is conducted.

Figure 9 gives the set-up schematic and the oscilloscope traces of monitor detectors output. The scope trace shows two curves. Upper trace is from the input power monitor detector which gives a step function denoting the application of laser to the SPPC mirror, t=0 point. The lower trace is the SPPC beam monitor detector output showing the gradual increase of the SPPC beam output. The time constant T1 denotes the elapsed time when noticeable SPPC output occurs. Another time constant T2 denotes the elapsed time when SPPC output reaches about 50% of saturation level. (It was noticed that there may be another slower time constant since the apparently saturated SPPC output continues to rise to a level higher than R.)

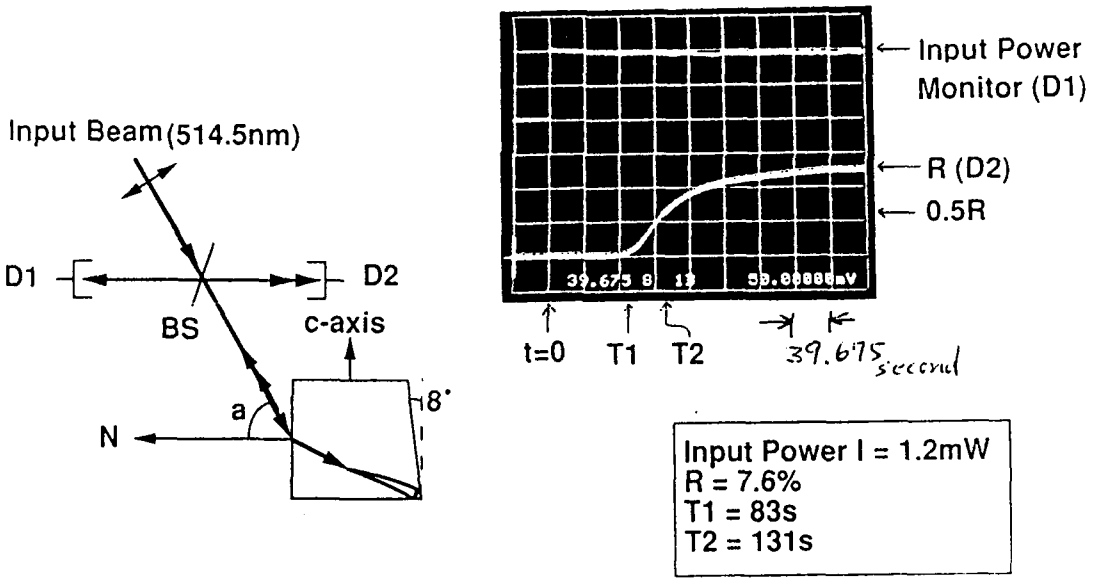

Figure 9, Experimental Set-up and Time Response Notations.

When the 514.5 nm laser input power is set at 2.4mW, the time response, T1, and the saturation phase conjugation reflectivity, R, are measured as function of the laser incidence angle, "a". After each measurements, the phase conjugate mirror inside the crystal is erased by flooding with strong laser beam while rocking the crystal. The angular response data are plotted in figure 10. Note that a sharp minimum of time constant T1=14.4 sec occurs at 60 degree incidence angle which also corresponds to the maximum point of SPPC reflectivity, R=12.4% with the 2.4 mW laser beam.

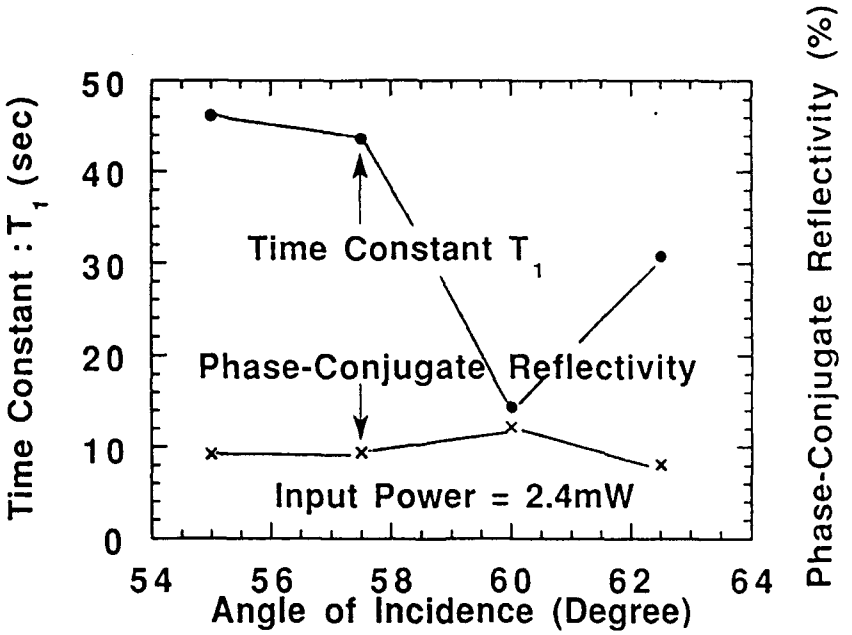

Figure 10, Angular Response of SPPC Mirror at 2.4 mW 514nm Radiation.

Next, the SPPC crystal and laser beam are set at 60 degree incidence angle while the laser power is adjusted. The data shows a minimum SPPC activity at 0.18 mW of laser power and that the SPPC beam appears at T1=522 second or less than 9 minutes, and it reaches 50% of saturation at T2=792 seconds or about 13 minutes. The saturation efficiency observed is more than 7.2%. The time constants shortens as laser power increases. When the laser power is increased to 28.6 mW, the measured response times are T1 = 4.2 second, and T2 = 19.6 second. These data is plotted in figure 11. It appears that further reduction of response to under 1 second may be possible with more than 100mW of laser power.

In another experiment for the purpose of finding out the saturation SPPC efficiency an electro-optic modulator is inserted into the input laser beam path as shown by figure 12. Since the SPPC is based on intensity exposure, intensity modulation of the laser beam will not affect the SPPC mirror process other than slow it down due to reduced average intensity.

The SPPC output beam now carries the modulation waveform and can be compared on oscilloscope. When the SPPC efficiency is still rising, the SPPC output beam waveform slope, which is proportional to SPPC beam intensity, continues to increase as shown by figure 13. Eventually, the SPPC efficiency stops at saturation level and the SPPC output beam waveform slope no longer changes as function of time, see figure 14. The saturation SPPC efficiency is measured about 15.7% which is higher than all the apparent saturation values, R, in previous figures.

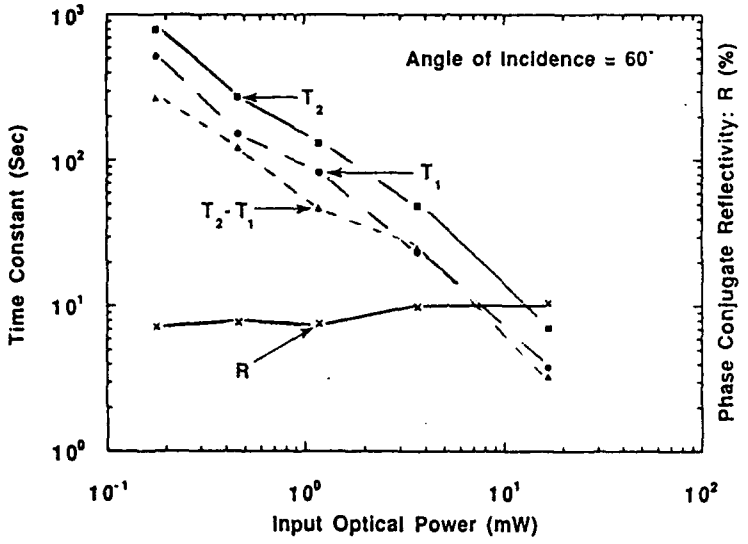

Figure 11, Response Time of the SPPC Mirror at Optimal Angle Setting as Function of Input Laser Power at 514nm.

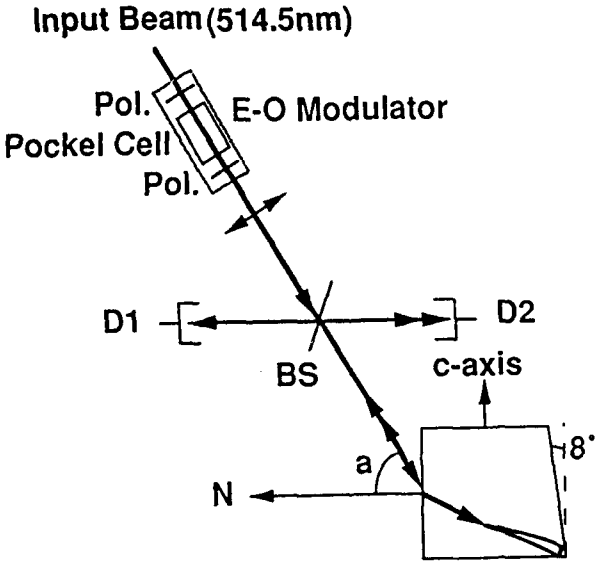

Figure 12, Insertion of Electro-Optic Modulator into the SPPC Experimental Set-up.

These experiemental results are very encouraging in terms of SPPC sensitivity and efficiency for the sake of demonstrative experiments for the intended fiber optical application. The response time of a few seconds is a little slow but still workable. Thus, the experiments shall be continued to include the use of a piece of optical fiber in the optical path.

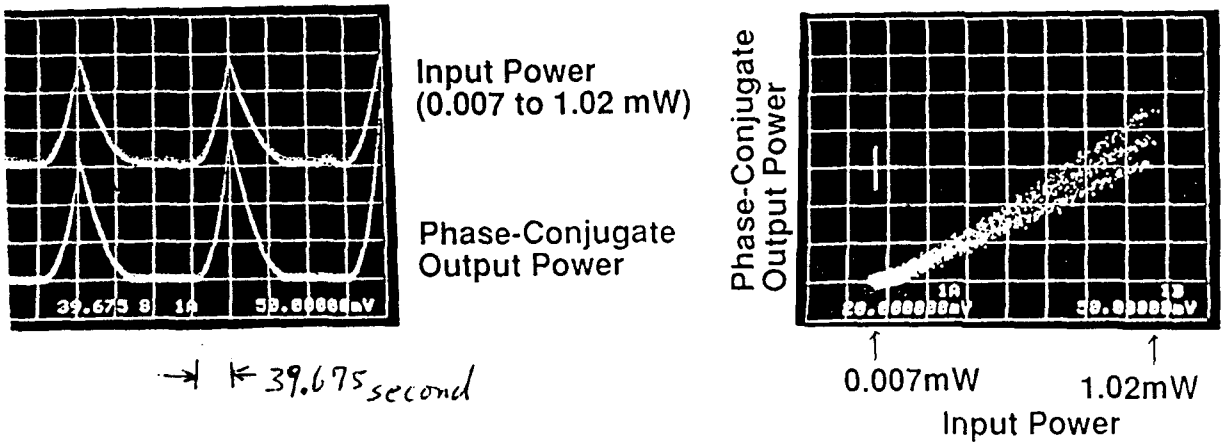

Figure 13, Traces of SPPC Output Beam Slope When Efficiency Still Rising.

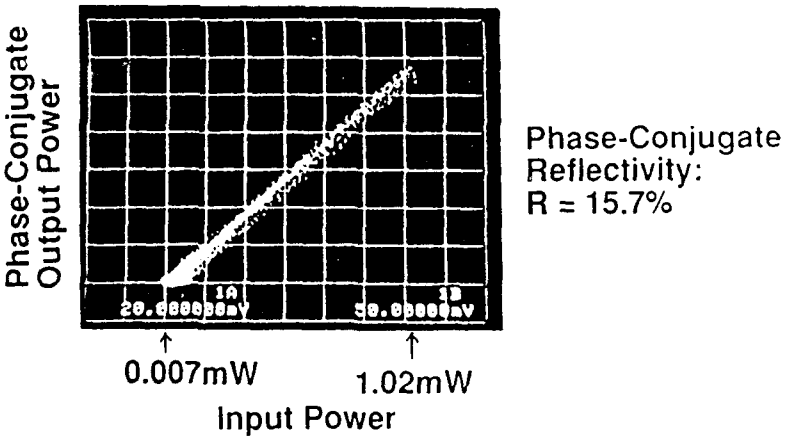

Figure 14, Traces of SPPC Output Beam Slope When Efficiency Stops Rising.

4.5 EXPERIMENTAL OBSERVATIONS WITH THE KITTY ARRANGEMENT:

4.5.1 EXPERIMENTAL SET-UP: The laser line used for this experiment is the green 514.5 nm line purified to single longitudinal mode operation using an intra-cavity etalon.

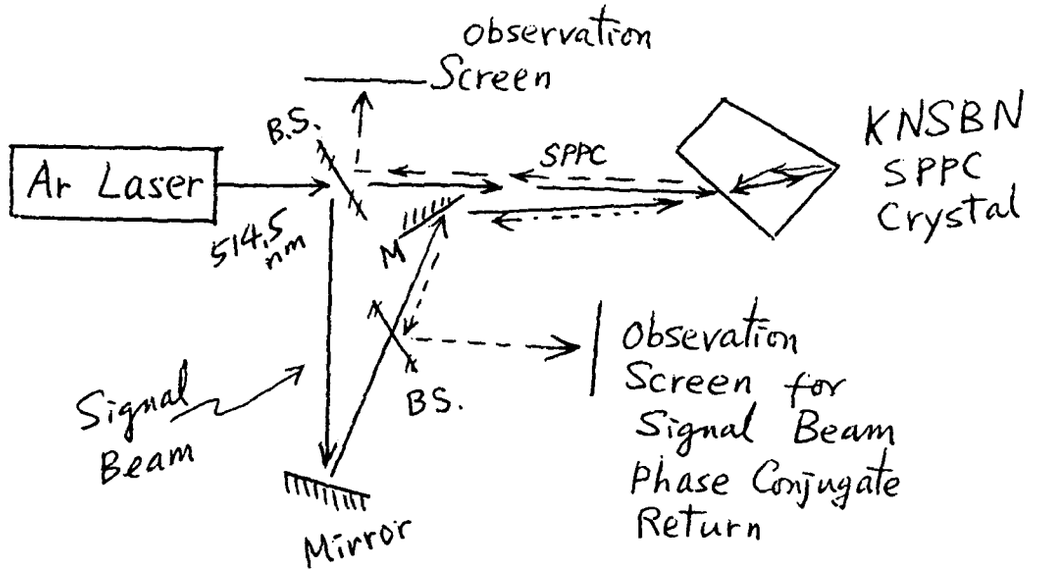

Figure 15(a) "KITTY" Arrangement for Phase Conjugate Reflection of a Weak Signal Beam.

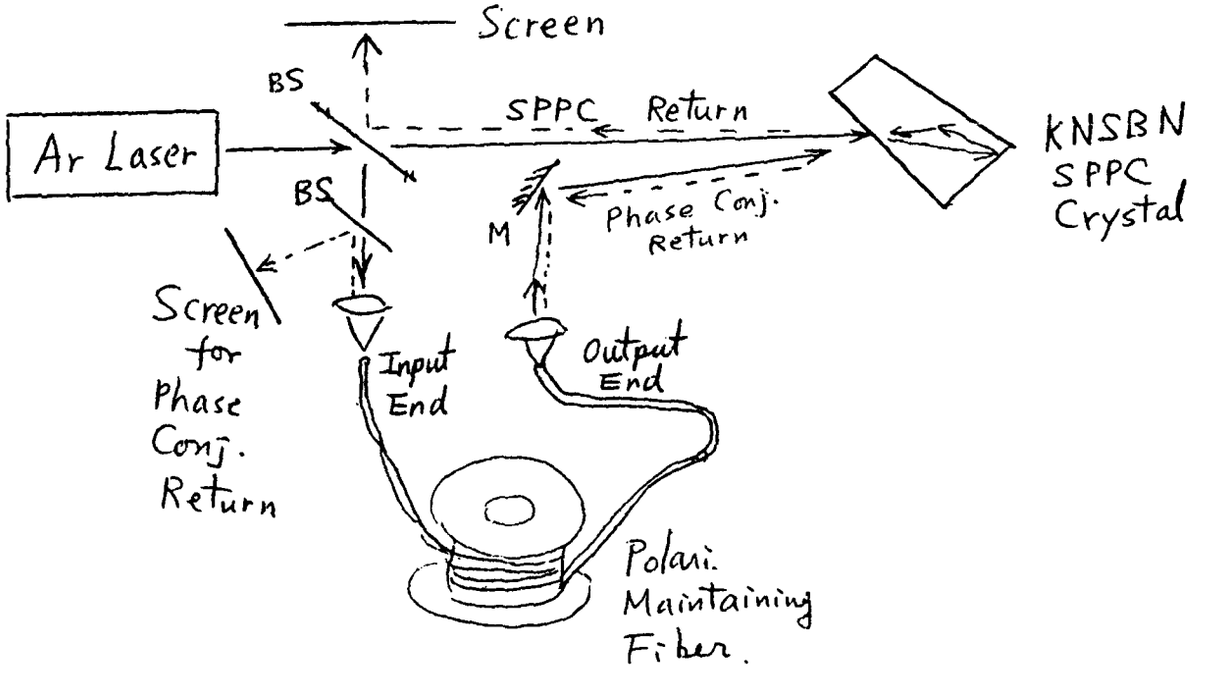

Figure 15(b) "KITTY" Arrangement for Phase Conjugate Reflection of Fiber Optical Signal.

The experimental set-up is the "KITTY" arrangement as shown by figure 15. The KNSBN photorefractive crystal is used in a "CAT" arrangement as Self-Pumped Phase Conjugate (SPPC) Mirror with the 514.5 nm laser beam entering the crystal at about 62 degree incidence angle. This strong laser beam (pump) will act to assist the SPPC activity for much weaker signal beams.

To facilitate the KITTY experiment, a small portion of the laser beam is diverted by a variable beam splitter mirror to a loop path of mirrors and beam splitter. The much weaker signal beam is also sent to the KNSBN crystal making an angle of about 5 degree to the main beam (the assisting laser beam). In this arrangement, the SPPC reflectivity of the weak signal beam can be enhanced by the presence of the much stronger main beam for higher reflectivity and faster response time.

For observation of the SPPC reflection of the pump beam, a screen is placed near the variable beam splitter mirror for intercepting the colinear reflection from the KNSBN crystal. The same beam splitter is not useful for monitoring the phase conjugation reflection of the signal beam since the screen will be in the way of the laser input beam. A second beam splitter mirror as well as a screen is placed in the optical loop of the signal beam for monitoring the KITTY reflection.

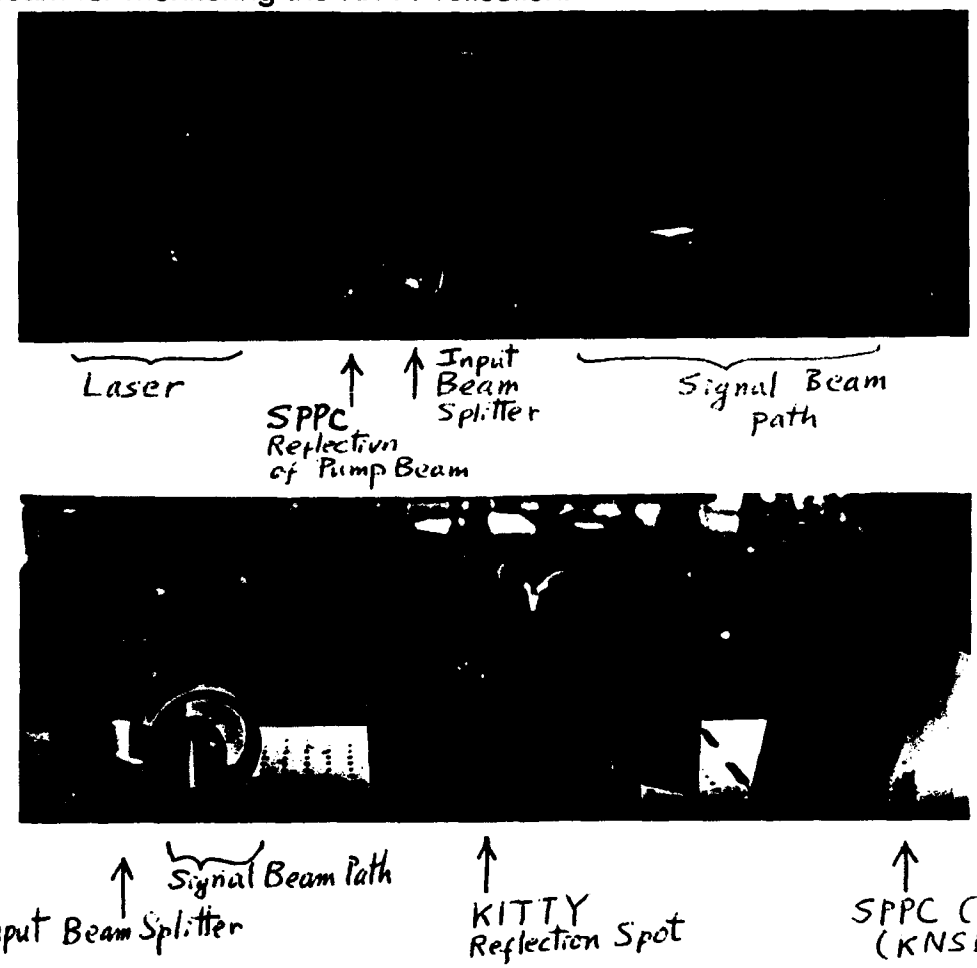

Figure 16, (a) The SPPC reflection Spot of the Pump Beam, and (b) the KITTY Reflection Spot of the Signal Beam.

4.5.2 EXPERIMENTAL OBSERVATIONS:

In the experiments, we obtained the SPPC mirror reflection of the assisting laser beam (pump beam) by blocking off the optical loop of the signal beam. Within a second after the 514 nm laser beam is introduced to the KNSBN crystal, an extremely bright SPPC reflection spot appears on the screen near the variable beam splitter mirror. By rocking the KNSBN crystal, the response time is estimated about 1 to 1.5 second. The laser power in the SPPC input beam is approximately 60 mw, consistent with the SPPC characterizing data for 1 to 2 second response time. At such response time, slow phase drifts in the optical transmission medium can be tracked by the phase conjugation mirror while fast modulations in the form of optical intensity envelope (the RF data) will have no effect on the performance of the phase conjugation mirror.

Subsequently, the signal beam is introduced at about 5 degree separation to the stronger beam, well within the acceptance angle of the SPPC mirror of this KNSBN crystal. As soon as the signal beam is aligned to the KNSBN crystal its KITTY SPPC refection appears on the observation screen near the second beam splitter mirror. This spot is much weaker than the SPPC reflection of the pump beam since the signal beam is also much weaker.

We noticed the intensity modulation of the phase conjugate reflection of the signal beam as we perturb the optical path of the signal beam. This is due to phase changes in the signal beam due to optical path perturbation. The phase grating in the KNSBN crystal must be modified when the signal beam phase changes so as to provide phase conjugate reflections. The finite response time of the SPPC process causes the intensity modulation of the phase conjugate reflection of the signal beam. In the mean time, since the phase of the stronger beam is not perturbed, the SPPC reflection of the stronger laser beam remains steady.

The rise time of the KITTY beam is estimated by physically gating the signal beam with a beam block, and by insertion of a parallel glass slide into the signal beam optical loop. The parallel glass acts like a variable phase shifter to the signal beam simulating phase drift. Each time the signal beam phase changes, a new phase conjugation grating needs be generated inside the KNSBN crystal before the KITTY reflection can be produced. The response time of the KITTY device estimated by this method is also approximately 1.5 second.

Since the signal beam power is only about one milliwatt, normally we would expect the phase conjugate reflection to require many minutes to show a bright reflection according to the characterized data of SPPC reflections from this sample of KNSBN. The presence of the strong SPPC beam significantly increased the speed of phase conjugate reflection of the signal beam in the KITTY arrangement as expected. On the other hand, the finite rise time of the phase conjugate reflection of the signal beam is an indication that it is the phase conjugate reflection (the KITTY beam) instead of merely an instantaneous refection from the existing phase grating of the stronger pump beams.

4.6 EXPERIMENTS OF KITTY MIRROR WITH OPTICAL FIBERS:

In order to conduct the experiment with optical fibers in the loop, special fibers and lasers must be prepared including the polarization preserving fibers and the long coherence length lasers.

4.6.1 POLARIZATION PRESERVING OPTICAL FIBER:

In order to work with a phase conjugation mirror, the laser beams engaged must be able to form photorefractive gratings inside the photorefractive crystals. The photorefractive effect is a third order nonlinear optical phenomenon driving by optical intensity variations. Therefore, the pump laser beams must be able to form a periodical optical intensity distribution inside the crystal. For the case of a SPPC mirror, the initial SPPC grating is set-up from one laser beam, the polarization status is not really critical. The incident laser beam, the coner reflection beam, and the internal scattering seed beams are all at same polarization states; and there shall be no difficulty forming an interference intensity distribution. As photoconductive carriers are generated, dirfted, and trapped, a SPPC grating is formed inside the photorefractive crystal due to the electro-optic effect. The electro-optic coefficients are highly polarization specific and as a result the SPPC reflectivity becomes polarization sensitive.

For the KNSBN SPPC device, the largest electro-optic coefficients are r33=200, r13=50, and r42=850 in units of 10^{-12} m/v. Optical polarization parallel to the c-axis is preferred. In the KITTY arrangement intended for the RF phase noise compensation, the physical properties of the signal beam from the optical fiber are strongly influenced by the fiber. Careful selection of the fiber for experimental use is necessary.

Although phase conjugation can work with all modes from a multi-mode fiber, a single mode fiber is preferred for the sake of RF distribution bandwidth and dispersion considerations. Conventional single mode fiber actually supports two modes with orthogonal polarization. Due to fiber imperfections and environmental perturbations, the phase velocities of these two modes are slightly different sensitive to environmental perturbations such as temperature, pressure, bending and twisting. Since the two modes are polarization orthogonal, there is no interference between the two modes and the output intensity remains constant. However, the resultant polarization status of the fiber optical output is the joint effect of the two orthogonal polarization modes. Similar to optical propagation inside a birefringent medium, the optical output from a conventional single mode fiber will be elliptically polarized in general. Due to the long length of optical fibers, the polarization state of fiber optical output beam is highly sensitive to environmental perturbations and can be considered as random.

Polarization preserving single mode optical fibers has been available since the seventies using thermal stress birefringence to break the degeneracy of the two polarization modes in a single mode fiber. Commercial quality polarization preserving fibers are offered by Corning, ITT, Fujitsu, Andrews, and York. Polarization preserving fibers with single mode operation in the blue-green wavelengths is available from York. A 100 meter length of single mode polarization fiber operating in the blue-green wavelengths is obtained for the experiments.

4.6.2 LONG COHERENCE LENGTH AR ION LASER:

In preparing the experiments, we were concerned about the polarization and phase fluctuations due to the optical fiber transmission and the mutual coherence between the laser beam and the fiber optical output after a long delay distance due to the optical fiber. Using a polarization maintaining fiber controls the state of optical polarization. Using a more intense laser beam quickens the phase conjugate mirror process and allowing the phase conjugate mirror to track the phase fluctuation rapidly. In addition, long laser coherence length is required to assure mutual coherence of the fiber optical output and the laser.

In order to conduct this experiment, an Ar ion laser of relatively high power and long coherence length is desired. The coherence length must be several times longer than the length of fiber. The Ar ion laser we found for this experiment is a Spectra-Physics Ar ion laser capable of up to 5 watts of output. Use of a powerful laser allows the incorporation of an intra-cavity etalon which selects a single longitudinal mode out of the large number of modes in the 514 nm wavelength band. With the mode selecting etalon, the 514 nm laser power is reduced to merely about 100 mW. But, the laser linewidth is in the order of 1 MHz providing sufficient coherence length for the includsion of optical fiber in the phase conjugation experiment.

4.6.3 THE FIBER IN THE LOOP SPPC AND KITTY EXPERIMENTS:

The optical set-up is illustrated by figure 15 (b) with a photograph. A 20 meter length of single mode 514 nm wavelength polarization maintaining optical fiber, which was bought from York, is inserted into the optical path of the signal beam of the SPPC-KITTY set-up of figure 15 (a). Care is taken in alignment of the optical polarization to the birefringent axis of the polarization maintaining fiber. When alignment is made, the optical polarization of the output beam after transmission through the fiber shall become insensitive to temperature and uniform-pressure perturbations applied to the fiber.

To observe the KITTY reflection with fiber in the loop, two beam splitters were inserted into the loop, one at each end of the fiber. The beam splitter near the output end of the fiber intercepts the KITTY reflection before it re-enters the fiber. The existence of this reflection proves the long delay path difference between the SPPC pump beam and the fiber optic signal beam does not has adverse effect on the operation of the KITTY device when a long coherence length laser is employed. Due to the relatively high coupling loss through the fiber (which can be improved in the future with better micro-manipulators) the fiber optical signal beam is very faint, less than 0.1 mw. According to earlier characterization of this KNSBN SPPC crystal, the minimum input light intensity level is 0.18 mw with a response time of 9 minutes. However, the observed response time of the KITTY reflection of the fiber optic beam remains at close to 1 to 2 seconds although the fiber optical signal beam intensity is now well below the minimum power needed for SPPC. This observation again verifies the desirable properties of the KITTY device for the proposed applications. Figure 17 shows the KITTY reflection for the fiber optical beam.

The KITTY reflection with optical fiber in the loop exhibits some intensity fluctuation

due to phase variations in the laser beam after transmission through the fiber which is sensitive to environmental variations. As we handled the fiber by hand, phase changes in the fiber optical beam rapidly and the KITTY reflection may disappear for a while. This observation prompted us to investigate into the phase change slew rate versus response time issue in the KITTY reflection mirror. Since the electro-optic phase grating will be completely displaced by half a cycle with a phase change of π in the signal beam, the allowed slew rate must be less than π/T1 rad/sec, where T1 is the response time, for tracking to occur. In this experimental set-up, this was verified qualitatively by heating the fiber with a hot air blower and watching the KITTY reflection spot. When the hot air is applied momentarily, the KITTY reflection disappear untill about 10 seconds later. Then it flickers slowly for a while before it becomes stabilized. This is to be compared with the observation of polarization mutation of the fiber optical beam while cooling when both polarization modes are launched. The polarization mutation slows to more than 5 to 10 seconds per cycle after 10 seconds of cooling from hot air.

KITTY reflection beam is also observed at the beam splitter near the input end of the polarization preserving fiber. This is significant because it is a good indication of the phase conjugation property of the KITTY reflection. Sending a laser beam over a distance of about 100 cm and coupling right back into the core of a single mode fiber (diameter about 9 micron) is a very difficult task using micro-manipulators. The fact that the KITTY reflection re-enters the fiber automatically is a clear indication of achieving spatial phase conjugation in the reflected beam. However, there seems some insertion loss in the process of about 4 dB, which is worth investigating about during the phase II program.

4.6.4 OBSERVATION OF THE PHASE NOISE COMPENSATED INTERFEROGRAM:

The KITTY reflection after retracing through the fiber should contain a conjugate phase of the incident laser towards the fiber. Note that the phase is referenced to the pump beam to the SPPC KITTY crystal. An interferogram is formed between the phase conjugate reflection and the incident beam by using a simple mirror in a Michaelson interferometer configuration of figure 18. The optical phase difference in the two beams forming the interferogram should be [(ϕr-ϕa)-ϕa], in which ϕr is the phase in the reference pump beam, and ϕa is the phase in the air path portion of the signal beam between the variable beam splitter mirror and the intercepting beam splitter. It is expected that the drift in the interferogram shall be mainly due to air turbulance in the beam path independent of phase drift in the optical fiber.

The observed interference fringes are very weak due to the faint KITTY return beam. However, the interferogram is stable, drifting only slowly. When the fiber is heated by hand touching, the interferogram either disappeared or flickered since the KITTY reflection disappeared sometimes. While flickering, the interferogram appears stable. The interpretation is that the flickering moments are when the phase change slew rate in the fiber is relatively high, faster than the response time of the KNSBN SPPC crystal at the pump beam power level. The stability of the interferogram during flickering indicates the independence of the interferogram from phase changes in the fiber as expected.

4.6.5 SUMMARY OF KITTY PHASE CONJUGATION MIRROR EXPERIMENTS:

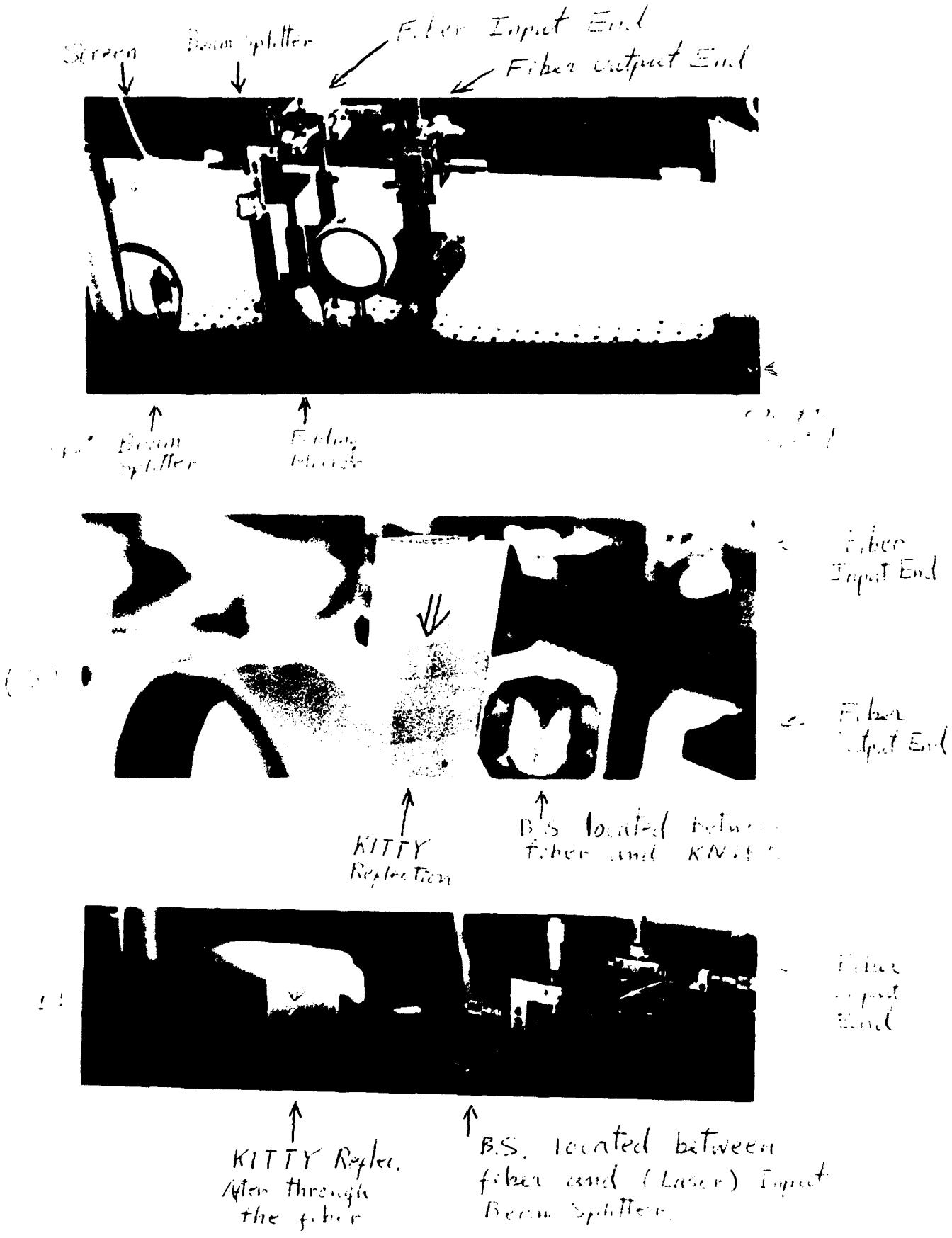

Figure 17, KITTY Reflection of the Fiber Optic Beam (a) Intercepted Before Reentering the Fiber, and (b) Intercepted After the Reflection has Retraced Through the Fiber.

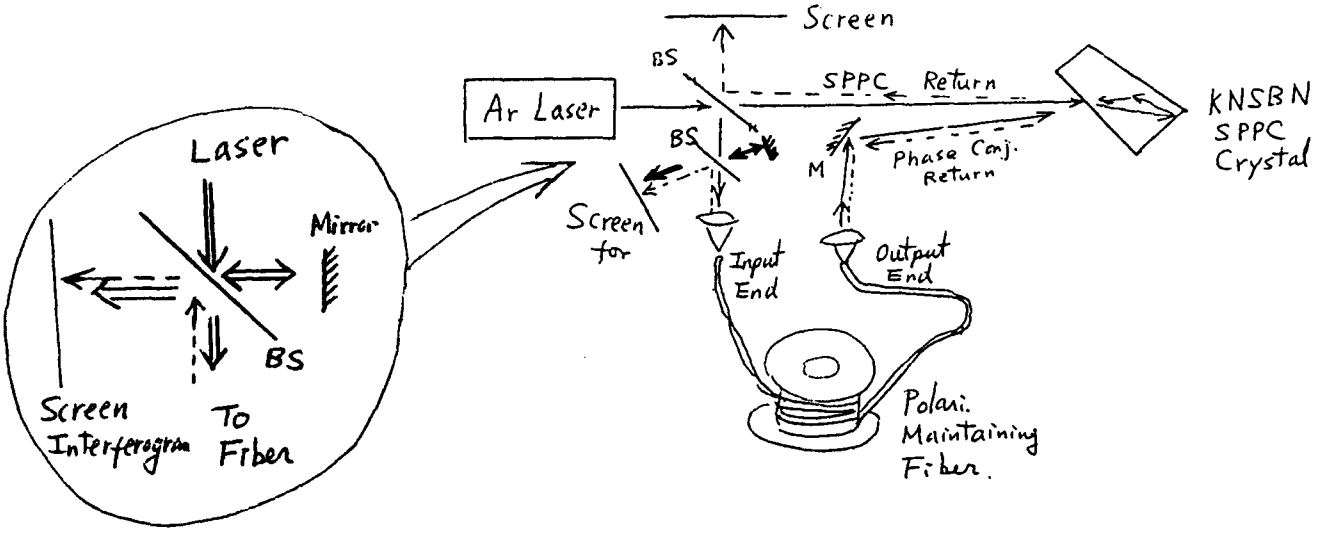

Figure 18, Optical Set-up for Observation of Interferogram between the KITTY Reflection and the Incident Beam to the Fiber.

The automatic alignment of the KITTY reflection back into the fiber verified that the KITTY reflection is spatially phase conjugate to the fiber optic siganl. The observation of stable interferogram at the input end of fiber independent of phase drift in the optical fiber verified that the KITTY reflection is also temporally phase conjugate to the fiber beam. Since the interferogram depending only on the phase drift in the air-paths, the phase drift in the air-paths can be measured by the interferogram set-up.

Comparing the experimental set-up with the proposed jitter free RF distribution link, the air-path in the signal beam between the variable beam splitter and the intercepting beam splitter simulates the RF transmission fibers from source to antenna elements. The optical fiber in the experimental set-up simulates the return fiber from antenna to the phase conjugation mirror near the source. The interferogram observed in this experiment simulates the output of the waveguide optical interferometer in the proposed system. As the interferogram in this experiment is dependent only on perturbations in the air-paths, ϕa and ϕr, we verified the principle of measureing the RF distribution fiber jitter by monitoring the output of the proposed waveguide optical interferometer.

4.7 DEVELOPMENTAL ISSUES AND RECOMMENDATIONS:

The ability to obtain true phase conjugation reflection for a very faint signal through an optical fiber marks a major milestone for the intended application. It assures the feasibility of the proposed approach for removing random phase jitter in RF distribution network. The remaining work are mainly device developments such as the SPPC Mirror crystal at laser diode wavelengths (GaAs, GaP or doped KNSBN), stable high power single longitudinal mode injection laser diodes and the waveguide servo-interferometer chips. These shall be recommended for phase II developments which islisted as follows.

1) Development of a Semiconductive SPPC KITTY device that operates at 0.68 to 1 micron wavelength range with high sensitivity, high efficiency, and high speed.

2) Development of a stabilized single longitudinal mode single transverse mode high power laser diode (200mw to 1 watt).

3) Development of the waveguide optics interferometer/phase shifter module for detection as well as compensating of phase drift in the RF distribution fiber.

4) Demonstration of the jitter free RF distribution link.

5.0 ULTRA HIGH SPEED SPATIAL LIGHT MODULATOR:

Spatial light modulator is a critical device which limits the performances of optical signal processing systems. Typical 2-Dimensional spatial light modulators available to date has good spatial resolutions up to 2000 x 2000 but relatively slow frame rate, in order of milli-seconds. A useful figure of merit for spatial light modulators is the resolution speed product. Current state of the art liquid crystal light valves has a figure of merit of approximately 2.4×10^8 pixel/second. An 8 element array of 1-dimensional acousto-optic spatial light modulators with 500 MHz bandwidth and 2 micro-second optical aperture can provide about 4×10^9 pixel/second with the frame rate in the order of 0.5 MHz.

For processing of phased array antenna signal of large number of array elements, the relatively slow liquid crystal light valves can be useful only as off-line processor. Conventional acousto-optic spatial light modulators have sufficient speed to carry the RF waveform from each antenna element in real time but is limited in forming only 1-dimensional arrays. A non-conventional acousto-optic spatial light modulator capable of forming 2-dimensional modulator arrays can offer fast frame rate 2-D spatial light modulation which is highly useful for optical processing of phased array antenna signal.

5.1 THE NOVEL DEVICE CONCEPT:

5.1.1 CONVENTIONAL ACOUSTO-OPTIC SPATIAL LIGHT MODULATOR:

Acousto-optic spatial light modulator is a mature technology[24-31]. In the conventional acousto-optic interaction geometry shown by figure 19, the acoustic field distribution along the X, Y, and Z directions can be imaged by an optical probe beam. Imaging of the acoustic field in the X-Y plane perpendicular to the optical probe beam is easily understood. At an arbitrary point on the X-Y plane, the incident optical ray will be diffracted according to acoustic field amplitude encountered. In a conventional 1-D acousto-optic SLM the X variation of acoustic field is transfered to the optical probe beam. Linear acousto-optic modulator array in the Y-direction has been constructed with up to 136 modulator elements[31] as page composer for optical recorders. However, it usefulness is limited in part due to the different physical properties (in terms of scale, pixel size, pixel refreshing rate, etc.) in the x and y directions. As a 2-D spatial light modulator, its effective frame rate will be realtively slow dictated by the acoustic transit time across the optical aperture window.

Assuming the phased array antenna of interest has 128 by 128 elements, and assuming a state of the art acousto-optic modulator element bandwidth of 512MHz,

refreshing 128 pixels along the acoustic propagation direction, X, requires 128/512 = 0.25 μs. Thus, the maximum frame rate of conventional acousto-optic SLM is less than 4 MHz. Although respectable, it is not fast enough for real time processing of the phased array antenna signal.

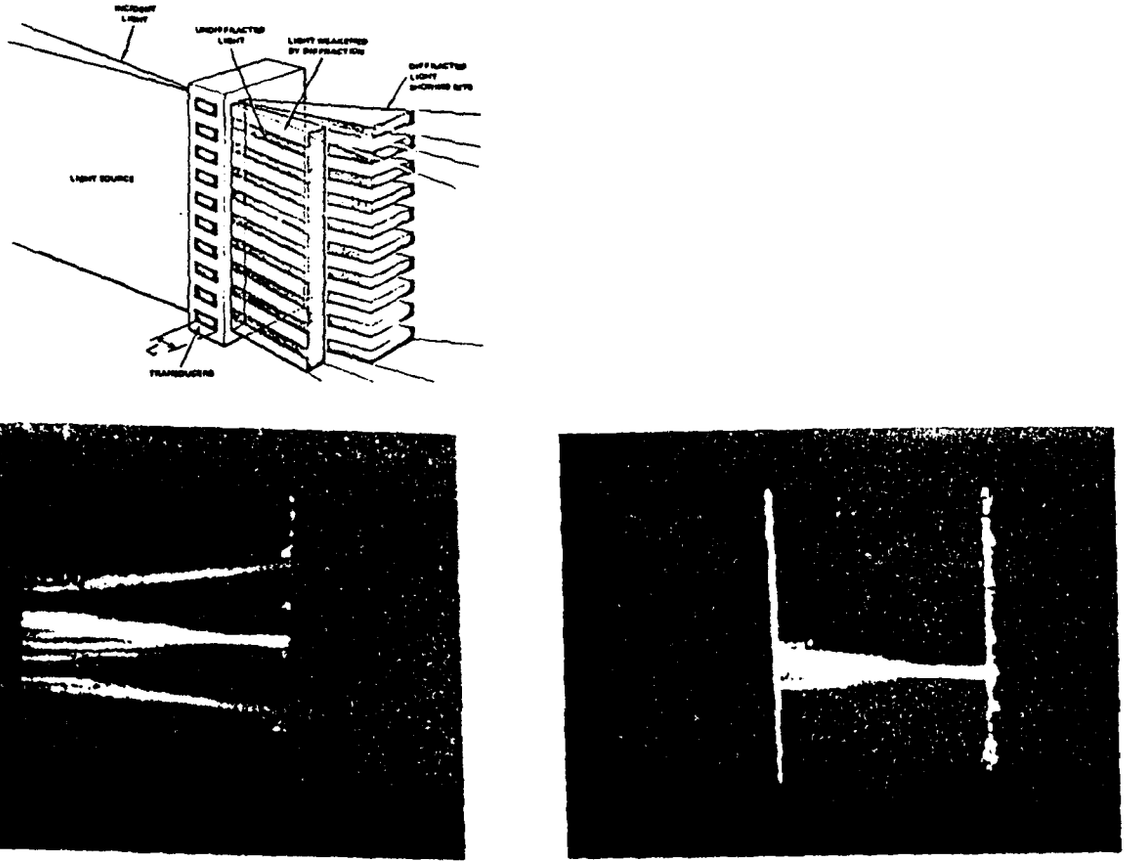

Figure 19, (a) Typical Acousto-Optic Interaction Geometry Showing Conventional AO-SLM, and (b) Focusing and Steering of Acoustic Field by Linear Acoustic Phased Array Probed by a HeNe Laser Beam (by the Author during 1976 while at Harris).

5.1.2 IMAGING ACOUSTO-OPTIC SPATIAL LIGHT MODULATOR:

In the proposed wideband 2-D acousto-optic imaging SLM, optical wavefront is modulated by acousto-optic imaging in the Y-Z plane using 2-D acoustic transducer array. The Z distribution of an acoustic wavefront can be transferred to the X-direction of the optical probe beam through an acousto-optic imaging process originally explored for imaging of acoustic fields for acoustic holography in the sixties and seventies.

Acousto-optic imaging differs from the common practices of acousto-optic modulation or beam deflection in such a way that the divergence angle of the optical probe beam is made substantially greater than the divergence angle of the acoustic field being probed. Momentum matching in the K vector space, see figure 20, transfers the amplitude and angular information of each acoustic vector, Ka, to a corresponding optical vector, Ko, of the incident optical beam. So long as the incident optical beam divergence angle

covers the range of acoustic beam divergence angle, the entire spatial spectrum of the acoustic field can appear on the optical wavefront. Thus, the Z-distribution of the acoustic field can be obtained by viewing the optical far field. Due to the much smaller optical wavelength comparing to acoustic wavelength, the optical image of the acoustic field will be reduced in size by the factor of Ka/Ko.

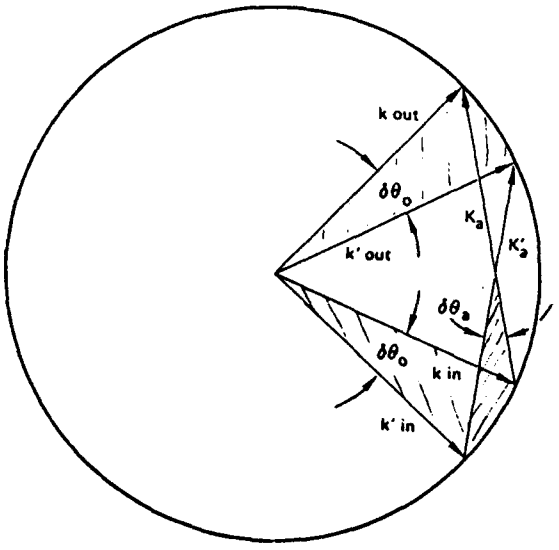

k in, k' in: INCIDENT OPTICAL WAVE VECTORS

k out, k' out: SCATTERED OPTICAL WAVE VECTORS

K_a K'_a: ACOUSTIC WAVE VECTOR

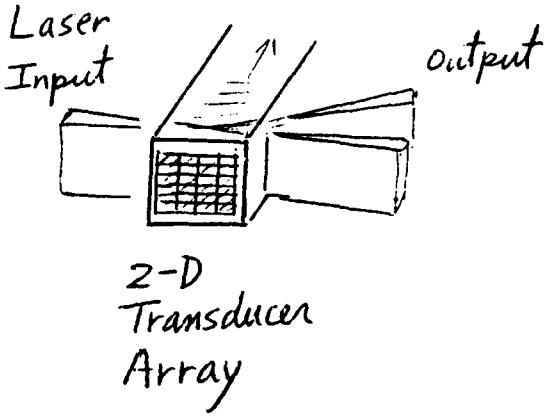

Figure 20, (a) Acousto-Optic Momentum Matching Diagram for the Case of A-O Imaging, and (b) Acousto-Optic Imaging Wideband 2-D SLM.

In comparison, the optical beam divergence angle in a conventional acousto-optic modulator is substantially smaller than the acoustic beam spread angle. Only one particular spatial spectrum component of the acoustic field contributes to the acousto-optic process. This can be considered as imaging with extremely poor resolution such that the entire acoustic field distribution appears as one pixel.

Several device issues is investigated for potential applications in phased array signal processing, namely, frame rate, signal bandwidth, addressing of 2-D transducer array, imaging optics arrangement, resolution, and optical efficiency, etc.. Of vital importance is the frame and data rate. The three dimensional volume of the acoustic field can be considered as many antenna array frames stacked along the X-direction, the direction of acoustic propagation. To achieve high frame rate, the laser probe must be focused to a sheet beam going through just one of the many stacked frames. For instance, consider a data rate of 100 M-Samples/sec in a highly efficient GaP crystal, one data frame thickness is 64 micron which shall be the limiting width of the laser sheet beam. If we focus the laser beam to 50 micron, the depth of focus in GaP will be about 26 mm which is sufficient to arrange a large number of transducer elements in the Z-direction.

5.2 ANALYTICAL MODEL OF THE DEVICE:

The analysis emphasizes acousto-optic imaging along the critical z-direction since imaging along the other dimension, y, is considered trivial.

5.2.1 SIMPLIFIED THEORY: Acousto-optic imaging of acoustic field stems from early works in acoustic beam probing using laser beams[24]. It was found that the angular spectrum of the acoustic field becomes the dominating factor in the frequency response of the acousto-optic modulator[25]. Fourier optics theory[26] explains the relation of angular spectrum and imaging with the use of a simple optical lens. A comprehensive theory of two dimensional acousto-optical imaging was first developed by Korpel in the sixties which was applied to the field of acoustic holography by other researchers[27,28]. Instead of the tedious analytical treatments found in earlier analysis, a simplified model is given here based on known results from coupled mode equations for the acousto-optic interaction.

Considering the case of Bragg diffraction with only one incident optical beam and one diffraction order, the wave equations subject to partial wave analysis (decomposing the optical wavefront into a summation of plane wave components) resulting in a set of two coupled mode equations.

$$\frac{\partial Uo}{\partial z} = \zeta\, U1 \qquad (1)$$

$$\frac{\partial U1}{\partial z} + i\,\beta 1\; U1 = -\zeta\, Uo \qquad (2)$$

where

$$\beta 1 = -\frac{K}{\cos\theta}\left(\sin\theta+\frac{K}{2k}\right) = -\frac{K}{\cos\theta}\left(\sin\theta-\sin\theta_B\right); \qquad \zeta = \left(\frac{\delta\epsilon}{\epsilon o}\right)\frac{k}{4\cos\theta} \qquad (3)$$

in the above equations Uo and U1 are the optical field in the 0-th order and the first order beams respectively, k and K are the wave vectors of the optical and acoustic waves respectively, θ is the optical incidence angle, θ_B is the Bragg angle, ϵ is the dielectric constant of the interaction medium, ß represent the phase mismatch between the coupled modes, and zeta represents the coupling strength. Since the incidence angle and Bragg angle are usually small, ß1 can be approximated by $K(\theta-\theta_B)$, which is proportional to the angular deviation of the incident laser beam from the Bragg angle, $\Delta=(\theta-\theta_B)$.

The solutions are exponential functions to be integrated along the interaction path. When the accustic field is uniform, the solution yields the well known sine and cosine terms for the 0th and the 1st diffraction orders. For the case of acousto-optic imaging of nonuniform acoustic field, the coupling strength, zeta, will be z dependent and the integration shall be carried out in detail. Such solutions are general and are valid for both weak and strong (when saturation may occur) interactions, and are for one plane optical wavefront component only.

However, in order to obtain good acoustic field image with fidelity, we are interested in weak acousto-optic interaction without saturation. Thus, the 0th order laser beam may be assumed un-depleted through the interaction region, and the 1st order laser beam can be obtained from just one of the equations, equation (2), with Uo being constant. The solution of U_1 has the general form of[29]

$$U1 \; - - \; Uo\, e^{-j\beta 1\, z} \int_{-\infty}^{z} \zeta(z')\; e^{j\beta 1\, z'}\, dz' \; - - \; Uo\, e^{-j\,K'\Delta z'} \int_{-\infty}^{z} \zeta(z')\; e^{j\,K'\Delta z'}\, dz' \quad (4)$$

Where $K' = K/\cos(\theta)$ is the projection of acoustic wave vector. The integral has the familiar form of fourier transform of zeta and denotes the angular spectrum of the acoustic field at a certain direction. Note that Uo denotes a plane wave component of the incident laser beam which is an angular spectrum component of the incident laser beam at a mismatch angle $\Delta = (\theta - \theta_B)$ from the Bragg condition. Therefore, the corresponding plane wave component, U1, of the diffracted light in the first order beam will carry a component of the acoustic angular spectrum, at anglular deviation Δ from the Bragg orientation.

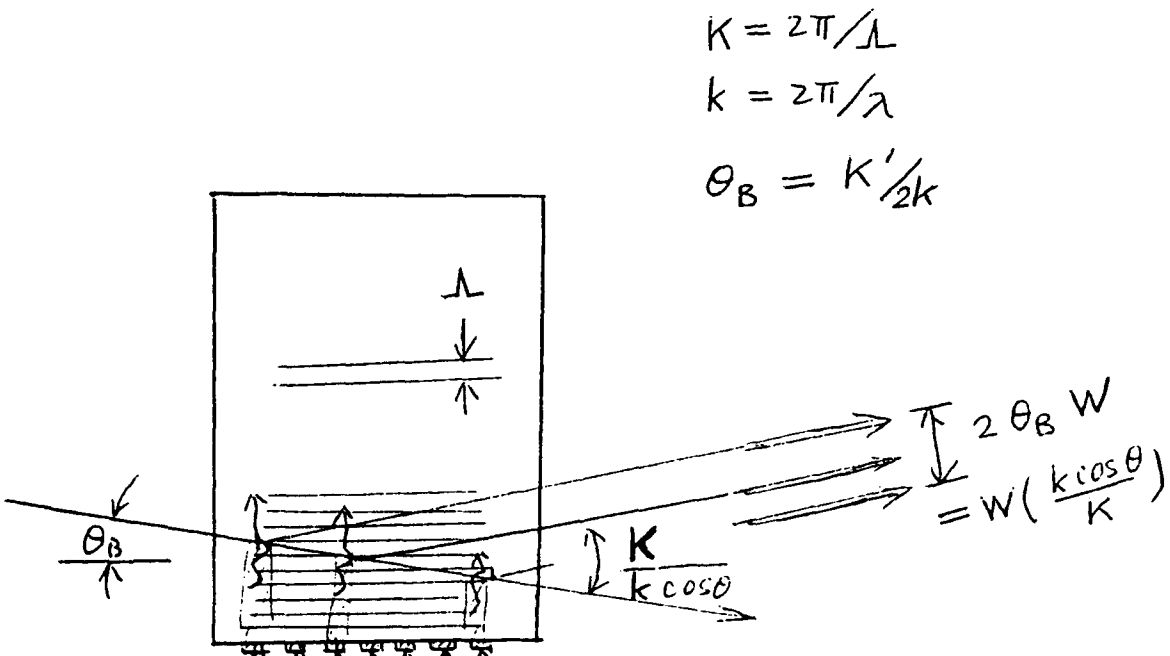

Figure 21, Ray Tracing Showing the Acousto-Optic Imaging of Acoustic Field.

The optical field, Eo, can be obtained by integrating the optical angular spectrum components, and is, when referenced to the Bragg angle,
Thus, if the input laser beam is focused containing a collection of tilted plan wave components over the numerical aperture of the focused beam, the entire angular spectrum of the acoustic field may be transferred to the angular spectrum of the diffracted

$$Eo \propto \int Uo(\Delta)\ e^{j\,k\,\Delta x}\ d\Delta \qquad (5)$$

first order laser beam as long as the angular spread of the incident light is greater than the angular spread of the acoustic field.

$$E1 \propto \int U1\ e^{jk\Delta x}\ d\Delta - \int Uo\ [\int \zeta(z')\ e^{jK'\Delta z'}\ dz']\ e^{jk\Delta x - jK'\Delta z}\ d\Delta \sim Uo\ \zeta(\frac{k}{K'}x) \qquad (6)$$

where a minute tilt of the propagation is ignored since $k >> K'$. As a result, the optical distribution in the diffracted order now images the acoustic field distribution with a scaling factor of ($k \cos \theta$ / K) which is the Bragg angle $\sin(\theta B) \approx \theta B$ and/or the optical to acoustic wavelength ratio. Such reduction in image size can easily be understood by simple ray tracing also, see figure 21.

5.2.2 PERFORMANCES OF ACOUSTO-OPTIC IMAGING DEVICE: Lets assume the acoustic velocity, Va, acoustic transducer element dimensions, dy and dz, acoustic frequency, fa, acoustic wavelength, $\cap a$, index of refraction, n, gaussian optical beam waist at e^{-2}, D, and optical wavelength, $\cap$. We have

Acoustic angular spread: $\cap a/dz = Va / (fa\ dz)$

Optical angular spread: $1.27 \cap / (n\ D) \geq \cap a / dz$

Optical aperture: $D \leq dz\ (1.27 \cap / n \cap a) = 1.27\ dz\ \theta B / n$

Optical focal depth: $2\ n\ D^2 / \cap$

Resolution Elements:
R = focal depth / dz
$\leq 2.54\ D\ \theta B / \cap$
$= 2.54\ D / \cap a$
$= (2.54/Va)\ D\ fa$

In comparison, a conventional 1-D acousto-optic SLM has resolution elements of (1/Va) D Δf, in which Δf is the acousto-optic modulator bandwidth usually less than 0.4 fa. Thus, the acousto-optic imaging SLM has the potential of more than 6 times higher spatial resolution for the same optical aperture size, D. Since the frame rate is limited by acoustic transit time across the optical aperture to Va/D, we arrive at a figure of merit, the resolution speed product RS = 2.54 fa for the acousto-optic imaging SLM. In comparison, RS = 0.4 fa for conventional 1-D acousto-optic SLM.

However, there are limitations. For large number of spatial resolution elements, D shall be made large and the physical size of the acousto-optic imaging SLM shall be matched to the near field distance (focal depth) of the laser beam for optimal performance. For slower devices with D greater than say 100 micron, the near field distance can be impractically long. Thus, acousto-optic imaging SLM is only practical

when D is small corresponding to extremely fast frame rate SLM devices.

Another important advantage of the imaging acousto-optic spatial light modulator is the shorter optical aperture D which reduces the negative effects of acoustic attenuation as well as acoustic diffraction. Devices working at much higher acoustic frequency with acoustic attenuation approaching the range of 100 dB/cm is theoretically possible with the acousto-optic imaging SLM.

From the above analytical results, we notice that acousto-optic medium that can support high acoustic frequency with slow acoustic velocity is preferred for the sake of resolution and physical size considerations. Note that, for given resolution, R, the physical size of an optimized device is

$$\text{Size} \geq 0.31 \ (n \cap a^2 R^2) / \cap$$

Small sized device is preferred favoring longer optical wavelength operation in lower index of refraction medium with short acoustic wavelength (slow acoustic velocity).

The frame rate of these SLMs will be extremely fast given by the acoustic transit time, Va/D = 2.54 fa/R which is proportional to acoustic frequency divide by resolution. Fast frame rate SLM must operate at high acoustic frequencies.

5.2.3 THE DESIGN RULES: The design starts from finding the most desirable materials and optical wavelength. The resolution is proportional to the product of optical aperture and acoustic frequency which are both design parameters. The frame rate, Fr, is proportional to the acoustic frequency divided by the resolution. In other words, the acoustic frequency shall be set by system requirements, resolution and frame rate as

$$fa = 0.394 \ R \ Fr$$

For example, if resolution R = 128, and frame rate Fr = 100 MS/s, the acoustic frequency must be higher than 4.9 GHz. The design constraints are physical size of the device, the optical wavelength of choice, and the desired SLM resolution. A list of possible designs are given as follows

	Velocity	fa (100dB/cm)	Limit Wavelength	M2
TeO2 Longi	4.2 μm/ns	about 3 GHz	1.4 μm	34
Fast Shear	2.1	about 5 GHz	0.42 μm	---
Slow Shear	0.62	about 0.6 GHz	1.03 μm	790
GaP Longi.	6.32	about 10 GHz	0.63 μm	45
Shear	4.1	about 20 GHz	0.21 μm	41
BGO Shear	1.77	about 6 GHz	0.3 μm	9

Optical wavelength (the longer the better): 0.9 μm or 1.3 μm

Since shorter acoustic wavelength is preferred subject to achievable acoustic frequency, the preferred materials are the slow shear wave in TeO_2, the fast shear wave in TeO_2 or the shear waves in BGO. The corresponding acoustic wavelengths will be 1 μm, 0.42 μm and 0.36 μm respectively.

Using the suggested device materials, the physical size of the SLM will be

$$\text{Size} \geq 0.31 \ (n \cap a^2 R^2) / \cap$$

For the example of resolution R=128 elements, optical wavelength $\cap$=0.9 μm, the device size will be approximately 13 mm for the slow shear wave TeO_2 design, 2.2 mm for the 5 GHz fast shear wave TeO_2 design, and 1.7 mm for the 5 GHz BGO shear wave design.

The optical aperture, D, is obtained from

$$D = 2.54^{-1} \cap a \ R$$

and will be 30.6 μm, 21.2 μm, and 18.2 μm respectively. The transducer element size, dz, will be simply the physical size divide by the resolution, R, and will be 100 μm, 17.2 μm, and 13.3 μm approximately for each of the examples.

The frame rate of these SLMs will be extremely fast given by the acoustic transit time, Va/D = 2.54 fa/R. For the above three examples, the limiting frame rates will be 12 MHz, 100 MHz, and 100 MHz respectively.

Considerations on diffraction efficiency and drive power requirement depends on application. The phased array antenna processor expects the coherent summation of all array elements to a focal point when certain RF source exists. Processor signal to noise ratio will be enhenced by the huge spatial compression gain (focusing). For the case of 128 elements (in one of the 2 dimensions), the focused intensity gain will be $(128)^2$ = 16,384 or 41 dB which must not be allowed to deplete the incident laser beam. Thus, the RF power requirement is for one row of array elements to work coherently for an acousto-optic diffraction efficiency of say 5% (much less than 50% to stay in the linear range). Assuming the transducer array element size dy, dz of 100 μm by 13 μm for a BGO device, the 128 element row will be about 100 μm by 1664 μm, and the RF drive power needed will be only 74mW/128 = 0.58mW per element for 5% maximum efficiency.

If instead of BGO, GaP or slow shear wave TeO_2 devices are considered, the RF drive power per element will be as small as 1.24mW/128 = 97 μW per element or 0.11mW/128 = 0.86 μW per element respectively. Such low RF drive power will be a major feature of the proposed acousto-optic imaging SLM for phased array antenna.

It is interesting to compare the performance of one row of the slow shear wave TeO_2 acousto-optic imaging SLM with 1-D acousto-optic SLM of conventional approach. In order to design a fast 12 M-Frame/s 128 pixel acousto-optic SLM, a GaP device

operating at 2.5 GHz center frequency with 1.5 GHz bandwidth and 83 ns optical aperture shall be used. Acousto-optic spatial light modulators of such performances is current state of the art and has been demonstrated for radar warning receiver type of applications with about 10% diffraction efficiency per watt of RF drive power. For one row of 128 element acousto-optic imaging SLM, total RF drive power will be 0.11 milliwatt for 5% diffraction efficiency as compared with 500 milliwatt for state of the art acousto-optic SLM of conventional design.

The reason why we propose to operate in the high linearity acousto-optic region of 5% diffraction efficiency is as follows. When the antenna field consists of radiation from multiple radiators, the acoustic field of each element in the acousto-optic imaging SLM will be the superposition of multiple phased waveforms of multiple frequencies. Consider the components of same frequency but from different source location, the component fields from the array elements will be modulated due to interference. The non-uniform acoustic field will be faithfully imaged optically and the angular spectrum of the non-uniform field will reveal the multiple emitter sources. Obviously, linearity is crucial to keep spurious intermodulation products minimal.

5.3 EXPERIMENTAL RESULTS:

5.3.1 OBSERVATION OF SPATIAL FEATURES BY IMAGING ACOUSTO-OPTIC SLM:

The acousto-optic imaging spatial light modulator theory is verified experimentally using a commercial two element PbMoO4 acousto-optic modulator and a special two element slow shear wave TeO2 beam deflector. Note that in either one of these two single-channel acousto-optic devices, two acoustic transducer elements are in tandem along the laser beam path. We demonstrated that in case of the PbMoO4 modulator, the two element acoustic field is imaged with the tiny gap between elements unresolved, while in case of the TeO2 device, the two well separated active element acoustic field as well as the wide gap (can be considered as three pixels, two ON and one OFF) is well resolved by acousto-optic imaging.

Case 1, PbMoO4 modulator: The transducer of this modulator has two elements in close proximity to each other. As a laser modulator, the laser beam goes through the acoustic field of both transducers while the acousto-optic interaction due to the second transducer element further enhances the acousto-optic diffraction due to the first element. Since in conventional optical setup the laser beam, although focused for the sake of modulation speed and rise time, has its beam divergence angle much smaller than the beam divergence angle of the acoustic field, the effect of two acoustic transducers is not noticeable. This modulator has the following physical parameters

Operating frequency range:	60 to 120 MHz
Transducer elements:	two
Transducer element size:	8 mm each
Gap between elements:	1.5 mm approximately
Acousto-optic material:	PbMoO4

The intended experiment is to arrange the laser beam and the acousto-optic experiment for acousto-optic imaging of the two element acoustic field. In other words, we want to observe the deterioration of the acousto-optic modulator output laser beam quality due to the non-uniform acoustic field. We shall focus the laser such that the laser beam divergence angle exceeds the acoustic beam divergence angle of each acoustic transducer elements. However, as the laser is focused tight, the beam divergence angle can approach the Bragg diffraction angle, $2\theta_B$, and the diffracted beam will overlap the un-diffracted beam. Thus, it is necessary to keep the acoustic frequency sufficiently high so that the diffracted beam can stay outside the un-diffracted beam, unless abnormal Bragg diffraction with polarization rotation is employed.

Diffracted beam angle: $2\theta_B = \cap/v\ f$
Minimum optical divergence angle: $\delta\theta_o = n\,v\,/\,(d\,f)$

where n is refractive index, v is acoustic velocity, $\cap$ is optical wavelength, d is transducer element size, and f is acoustic frequency. The acoustic frequency must be kept higher than the intersection of the two curves as shown by figure 22. That is

$$f > v\ \sqrt{(n / \cap d)}$$

Thus there exists a minimum acoustic frequency which is proportional to the acoustic velocity. For example, in a PbMoO4 device, v = 3.6 mm/μs, n = 2.4, and if using HeNe laser with $\cap$ = 0.633 μm, the acoustic frequency must be higher than 78 MHz for transducer element size of 8mm each, and higher than 156 MHz or 312 MHz for transducer element size of 2mm or 0.5mm each respectively.

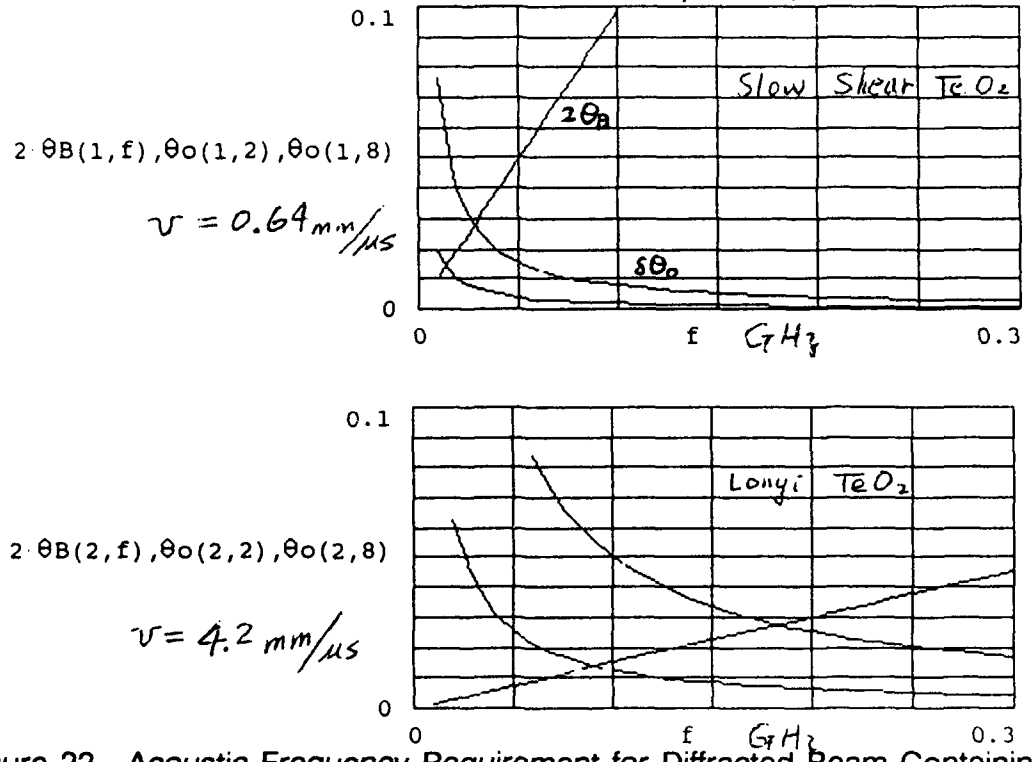

Figure 22, Acoustic Frequency Requirement for Diffracted Beam Containing Acoustic Field Image to be Angularly Separated from the Un-diffracted Beam.

Operating at the higher frequency end of the modulator transducer response, the laser beam focusing condition is derived as follows

Acoustic wavelength at 120 Mhz:	3.6 μm/ns / 0.12 GHz = 30 μm
Acousto-optic diffraction angle:	0.633 μm / 30 μm = 21.1 mR or F-47.4
Acoustic beam divergence angle:	30 μm / 8000 μm = 3.75 mR
Optical wavelength in PbMoO4:	0.6328 μm / 2.4 = 0.264 μm
Required optical spot size in PbMoO4:	< 0.264 μm / 3.75 mR = 70.4 μm
Focusing Beam F-number in air:	< 70.4 μm / (1.27 x 0.6328 μm) = F-87.6
Typical HeNe laser beam diameter:	0.65 mm
Focal length of lens:	< 87.6 x 0.65 mm = 56.94 mm

A microscope objective lens is employed with a negative lens of 25mm focal length to form a zoom system. The focusing F-number is easily adjustable over a wide range by changing the distance between the negative lens and the microscope objective lens. The resultant F-number can be estimated by observing the large projection of laser beam beyond focus. Such zoom system has the additional advantage of moving the focus away from the exit window of the microscope objective lens allowing ample working distance for the acousto-optic modulator alignment. The laser beam is adjusted to approximately F-50 which is sufficiently smaller than the maximum number of 87.6 providing uniform imaging of acoustic field, yet large enough for separation of the diffracted beam from un-diffracted beam.

When the optics is setup and the power turned-on a structured intensity distribution in the diffracted laser beam appears immediately. This pattern is given by figure 23, which is the far field of the acousto-optic image of the acoustic field pattern. It looks like a sinX/X pattern instead of a nominally circular (or sometimes elliptical) pattern in conventional acousto-optic modulator output. Now, we need only block the un-diffracted beam and focus the diffracted beam to obtain the image of the acoustic field.

However, the observed image of the two active acoustic elements appears as one larger element despite of careful alignments. The is due to insufficient spatial resolution for imaging of the 1.5mm gap between the two transducer elements. Referring to the discussion above, in order to resolve this 1.5mm gap the focusing optical beam must provide an F-number less than 0.264μm x (1600μm / 30μm)/(1.27 x 0.6328μm) = 17.52. The incident laser beam of F-50 is far too collimated for resolving the 1.5 mm gap.

Case 2, TeO2 beam deflector: The device used to be a single element acousto-optic beam deflector with diamond shaped electrode. However, it happens that a second transducer electrode were prepared on the piezoelectric transducer surface when the device was fabricated. It is possible to repackage the device with both of the transducer top electrodes electrically connected to become a two element array in tandem. The resultant device parameters are as follows

Operating frequency range:	50 to 100 MHz
Transducer elements:	two active

Transducer element size:	3.5 mm each, diamond shaped.
Gap between elements:	4.5mm or more due to diamond shaped electrode
Acousto-optic material:	TeO2, slow shear.

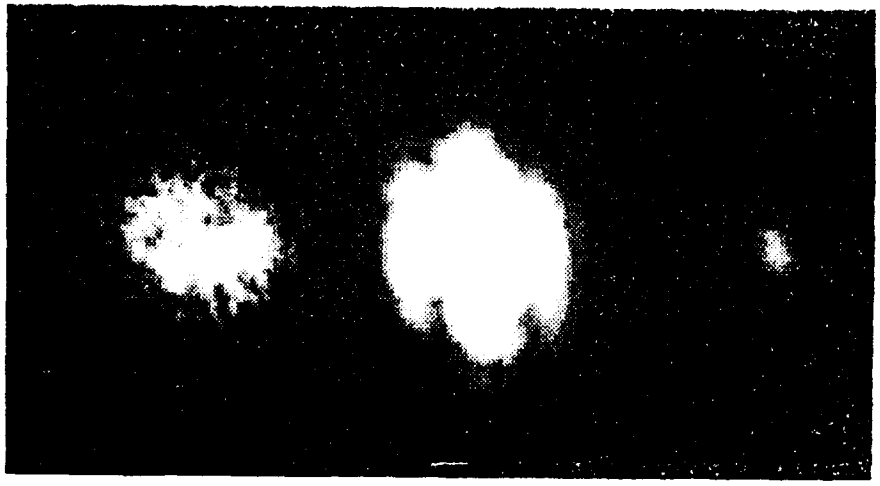

Figure 23, The Intensity Pattern in The Diffracted Laser Beam from the Acousto-Optic Imaging Experimental Setup with a Two Element PbMoO4 Modulator with Narrow Gap.

Apparently the gap for the TeO2 device is sufficiently big to be imaged together with the two active transducer elements. In fact, we shall consider this device a three pixel element array with two elements turned-on and the middle element turned-off. Note that due to the diamond shape electrodes, the dimension of the active elements and the dimension of the gap is variable by sending the laser beam through different part of the transducer height.

The acoustic frequency necessary for angular separation of the diffracted beam is now trivial. The optical focusing condition is as follows

Acoustic wavelength at 75 MHz:	0.65 μm/ns / 0.075 GHz = 8.67 μm
Acousto-optic diffraction angle:	0.633 μm / 8.67 μm = 73 mR or F-13.7
Acoustic beam divergence angle:	8.67 μm / 3500 μm = 2.48 mR
Optical wavelength in PbMoO4:	0.6328 μm / 2.4 = 0.264 μm
Required optical spot size in PbMoO4:	< 0.264 μm / 2.48 mR = 106.6 μm
Focusing Beam F-number in air:	< 106.6 μm / (1.27 x 0.6328 μm) = F-132.6
Typical HeNe laser beam diameter:	0.65 mm
Focal length of lens:	< 132.6 x 0.65 mm = 86.2 mm

Since angular separation of diffracted beam is trivial, we adjusted the zoom lenses to an F-number of 25 approximately. This F-number in input laser beam is twice bigger than the F-number of acousto-optic diffraction angle, more than sufficient for effective beam separation without using optical polarizers. Yet it provides five times more focusing than the minimum needed for acousto-optic imaging.

After the two active transducer elements are electrically connected, the acousto-optic diffracted beam exhibits a Young's interference pattern, see figure 24. Blocking-off the un-diffracted laser beam and focusing the diffracted beam for acousto-optic imaging yields an optical intensity pattern of two rectangles as expected, see figure 25. Note that we obtain rectangle instead of diamond shape because the focused laser beam is very thin sampling only a section of the diamond shape. Cylindrical lenses will be needed to provide a focused sheet beam for imaging of the diamond shape.

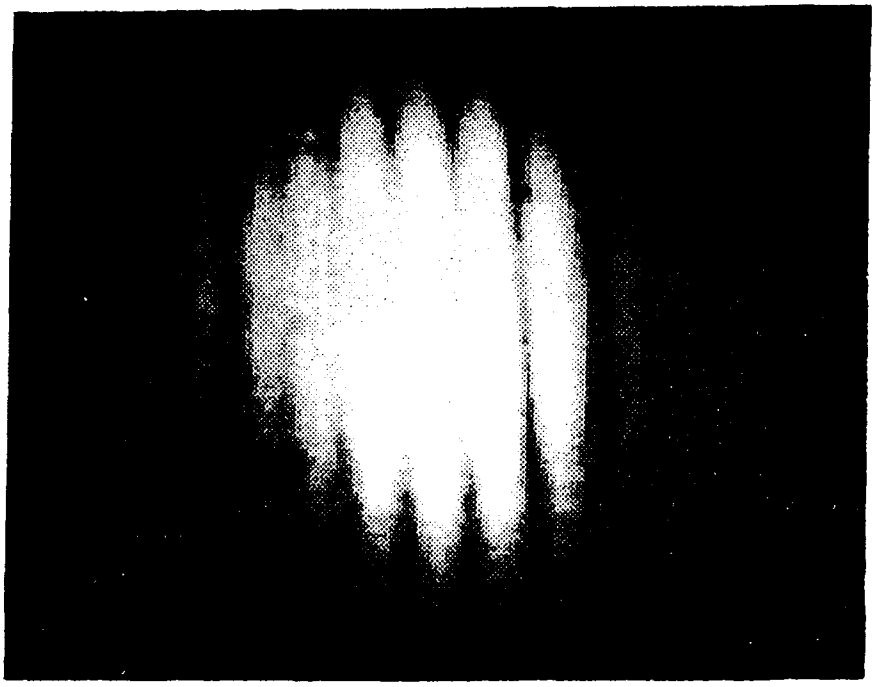

Figure 24, Young's Interference Pattern in the Diffracted Beam for Two Active Element Slow Shear Wave TeO2 Device with Wide Gap, Thus Three Pixels.

These experiments demonstrated the feasibility of acousto-optic imaging of acoustic field and verified the theory of acousto-optic imaging with tandem transducer array. The achievable resolution of acousto-optic imaging as function of the beam divergence angle of the optical beam is demonstrated. The speed of such acousto-optic imaging device shall be limited by the acoustic transit time across the tightly focused laser beam and by the bandwidth of the acoustic transducer.

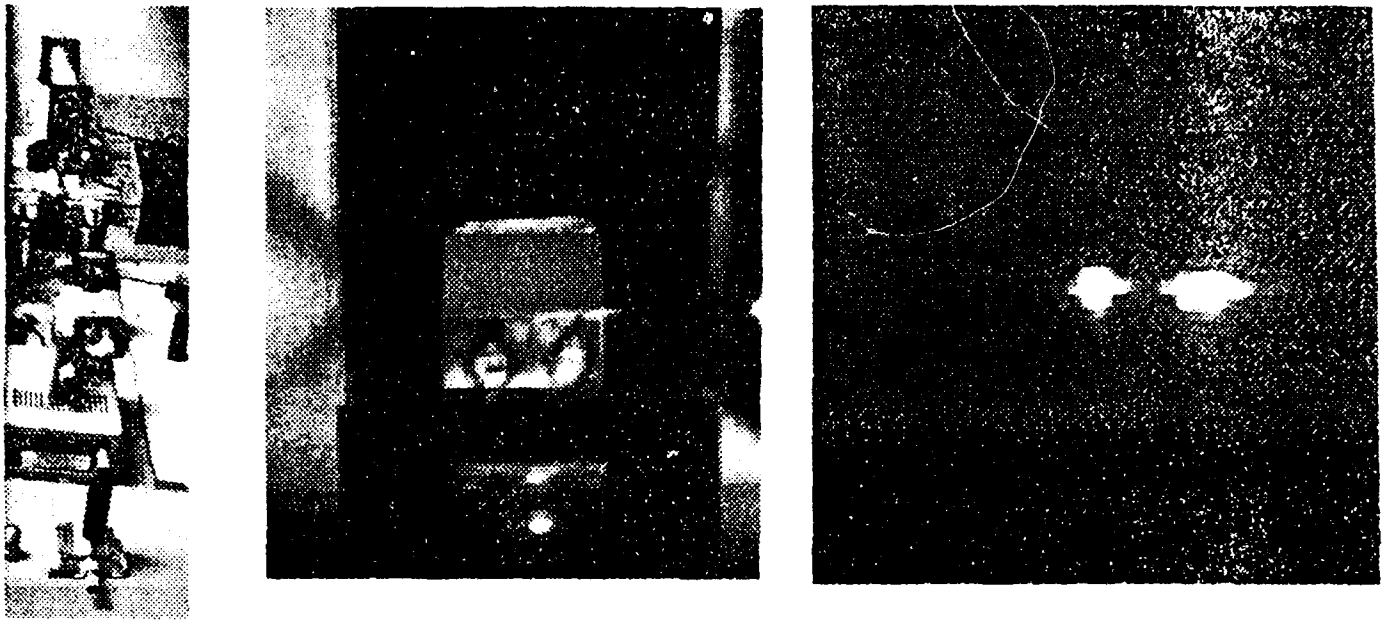

(a) (b) (c)

Figure 25, Acousto-Optic Image of the Two Active Element Acoustic Field. (a) Experimental Set-up, (b) The Two Element Transducer, and (c) Acousto-Optic Image of the Two Elements Using a Focused Laser Beam.

5.3.2 MODULATION SPEED OF THE IMAGING ACOUSTO-OPTIC MODULATOR:

The potential high modulation speed of these modulators have been verified experimentally by pulse modulation of the RF wavefront and detection of the deflected laser beam. For the PbMoO4 modulator with focused beam, the rise time is less than 25 ns. The slow shear wave TeO2 modulator is slower, less than 80 ns, due to the longer transit time for the acoustic beam to travel through the optical aperture.

From these experimental results, the resolution-frame rate product is $8x10^7$ pixel/sec and 37.5×10^6 pixel/sec for the PbMoO4 device and for the slow shear wave TeO2 device respectively. Since the depth of focus of the 0.65mm laser beams inside the crystals is approximately 3 meters, the device resolution-frame rate product can be made much larger than these demonstrated values by more than two orders of magnitude. Nonetheless, the 8×10^7 resolution-frame rate product of the demonstration using a make-shift imaging acousto-optic SLM is already equivalent to a rather advanced conventional acousto-optic sptial light modulator of 2 micro-second processing time and 160 pixels (or 80 MHz bandwidth).

5.3.3 SUMMARY:

Practical sized fast frame rate acousto-optic imaging SLM is feasible using microwave

acoustic transducers. Current demonstrated microwave acoustic transducer fabrication limit is in the range of 4 to 8 GHz. Therefore, the limitation on the resolution-frame rate products of an imaging acousto-optic SLM isabout 20 GHz. That is capable of providing 256 x 256 pixels at 80 Mega frames per second. Such a fast SLM would be extremely powerful for real time signal processing applications, if the data input addressing issue can be resolved. The salient features of the imaging acousto-optic spatial light modulator are

(1) For each material system, there is a minimum frequency for satisfactory SLM operation. This frequency increases as the acoustic velocity. For slow shear wave TeO2 devices, this frequency is less than 50 MHz, while for longitudinal TeO2 and most other devices this frequency will be above a few hundred MHz.

(2) The inclusion of bandwidth consideration yields a maximum frequency of operation which occurs when

$$f_{max} = L_{max} * \delta f / (L_o * 6.452), \quad \text{where} \quad L_o = 2 n v^2 / (\cap f \delta f)$$

Note that Lmax is the physical length of the acousto-optic transducer array dictated by the maximum size of crystal employed, and Lo is the characteristic interaction length of acousto-optic deflectors of center frequency f and bandwidth δf.

(3) The maximum number of resolution and thus transducer array element, is determined by the fractional bandwidth regardless of choice of material. For different material, this maximum resolution occurs at different frequency.

(4) For given material, the resolution of acousto-optic imaging SLM increases with decreasing fractional bandwidth.

5.4 DEVICE DEVELOPMENTAL ISSUES AND RECOMMENDATIONS:

The acousto-optical imaging array provides an opportunity to develop a wideband spatial light modulator (SLM) which can offer frame rate up to 5 to 6 orders faster than conventional 2-D SLMs (e.g. LCD, Magneto-Optics, Micro-Channel Plates, and Silicon Membrane). Figure 26 illustrates a design using parallel fiber optical addressing. Light is butt coupled to a matrix of high speed photoconductors deposited on the back of piezoelectric transducer platelet. Each photoconductor element is driven by optical signal waveform delivering an RF voltage on the transducer when light is on. Temporal spatial modulated acoustic wave will be generated from such array. The modulation speed is limited by the photoconductor rise and fall time, and the acoustic transducer bandwidth. Recent advances in opto-microwave interaction has demonstrated photoconductor speed in the pico-sec regime (ref. D.H. Auston, Picosecond Photoconductivity, Chapter 3, Semiconductor and Semimetals, Vol 28.) using impurity dominated or radiation damaged or polycrystalline or amorphous semiconductors. For the present application, back biased PIN array or deposited polycrystalline germanium (bandgap 0.85 eV) or deposited polysilicon (1.1 eV) are potential candidates. The acoustic transducer bandwidth depends on transducer center frequency and acoustic load. With carefully designed acoustic

interfaces, fractional bandwidth of greater than 70% on center frequency of up to 4 or 5 GHz is within limit.

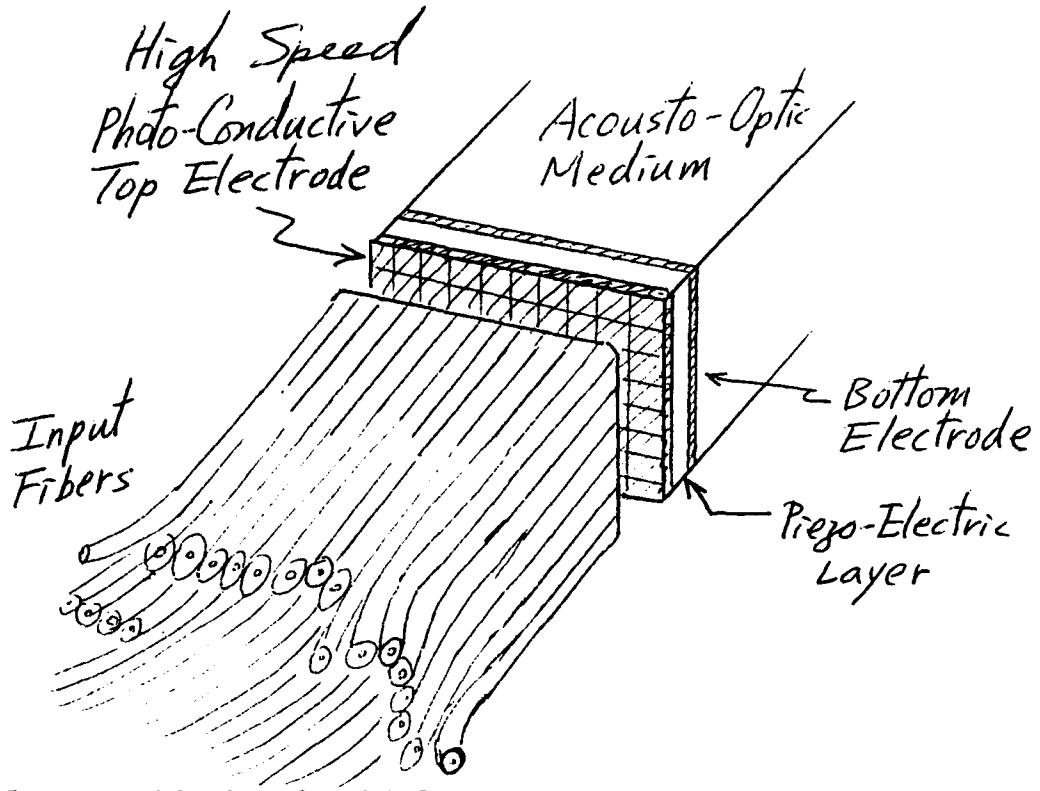

Figure 26, Conceptual Design of a High Speed Imaging Acousto-Optic Spatial Light Modulator Using Fiber Optic Addressing and high speed photoconductors.

6.0 PROCESSING OF PHASED ARRAY SIGNAL:

Many real time beam forming techniques have been reported[4-18,32,33] including fourier optical processors using ILD array, acousto-optic array, or 2-D spatial light modulators (SLM) for tap weight generation and acousto-optic correlation processors[34-38] with phtorefractive crystals or liquid crystal light valve for interference cancellation. One advantage of optical beam forming processors is the easy interface to an optical fiber distribution network for feeding the phased array antenna elements. These beam forming processors include (a) fourier transform processors for steering the physical antenna beams during transmission or the virtual antenna beams during receiving, and a family of very different processors (b) correlator adaptive loop processors for null steering and interference cancellation. The optical fourier transform processors first proposed by Koepf and others is based on fouier relationship between near field (antenna) and far field (destination) and is easily understood. We may consider the processor as optical or acoustic analogy of the microwave antenna.

The conventinal correlation adaptive loop uses Applebaum's model. It uses correlators to generate estimated signal (assuming of the spread spectrum type would be useful) and estimated interference or error in the phased array signal output port. The vector projection of estimated error in each of the array elements is calculated by means

of an acousto-optic correlator array, and feed to the corresponding array element as weight update increment. Physically, all these correlation calculations can be interpreted as looking for the amount of interference leak (cross-talk) of the interfering emitter through antenna sidelobe and the phase (or delay) factor at each array element due to the unknown emitter (direction finding). Such calculations should be possible using the fourier transform processor.

With the potential of an acousto-optic 2-D wideband SLM, real time fourier transform receiver becomes possible for phased array antennas. In real time fourier transform phased array receiver, the phased array behaves like a microwave lens and all emitters will be imaged on the receiver output plane. Phased array element weighing serves to (a) deflecting the microwave lens axis, or (b) introducing aberration adjusting far field pattern shape for null steering. The signal of interest appears as one pixel of the image and shall be correlated with its spread spectrum code for detection.

Like in the Applebaum model, the error waveform shall be produced by subtracting the estimated signal from the received antenna signal. The emitter sources for this error waveform can be found from the image plane. Correlating the error waveform with these emitter waveforms yields the interference contribution matrix (or physically, sidelobe contribution map). The cross-coupling sidelobes can be eliminated by forming a negating beam to the direction with opposite phase, i.e. sending weak beams toward the offending emitters to pick up some signal at negative polarity for adaptive cancellation. Therefore, the null steering mechanism can be performed in a beam forming processor capable of handling multiple beams. The above explanation indicates the possibility of using a fourier transform beam forming processor intended for trnasmitter weigh generation for the purpose of receiver interference cancellation.

6.1 NEW ADAPTIVE CANCELLATION PROCESSOR MODEL:

Null steering phased array processor based on Applebaum model has been the subject of intensive investigation during the recent years. An error signal is derived by subtracting the correlator detected signal from the antenna signal. Correlation of the error signal at antenna elements generates weight distribution at antenna elements for null steering. However, we believe a different approach can be formulated by correlating the error waveform at the focal image plane. Since locations on the focal image plane corresponds to angular location of RF sources, physical interpretation and null steering of the interfering signal may be more straightforward.

The following is a proposed approach for null steering. First, the error signal waveform is obtained just like in the Applebaum model approach. This step is necessary since otherwise the subsequent correlation will most likely be correlating the signal with its leakage into other focal plane elements. The coefficients for signal leakage to a specific location is not generally the same as the coefficient for interference signal from that specific location to the receiver. Such reciprocal relationship is true only when the antenna sidelobe (leakage) pattern is symmetric.

Next, the error waveform is correlated with signal received at the focal plane

corresponding to other source locations. The strength and phase of correlation between the error waveform and each source location is an indication of the amount and phase of interference from that source location to the receiver. The weights for each antenna element for steering the interfering source to the receiver can be calculated by Fourier transforming of the interfering source coordinate. The calculated weight vectors are subtracted to the existing weight vectors of the phased array. As a result, the receiver is tapping a fraction of the signal from the interfering source at negative polarity adding to the signal for interference cancellation.

The key device for this newer architecture is a multi-channel correlator for correlating the error signal with the source location map, i.e. focal plane array or far field of the phased array antenna. A 2-D high speed spatial light modulator array can be used to represent the received field from the phased array antenna. Optically transform the spatial light distribution yields optical field distribution at the source location map. The desired 2-D multi-channel correlation can be accomplished by modulating the light source with error waveform before going through the 2-D SLM, and by time integrating the resultant optical signal distribution with a 2-D CCD array. The 2-D CCD array output shall be related to the correlation of source locations with the error waveform.

6.1.1 SIGNAL PROCESSING USING IMAGING ACOUSTO-OPTIC SLM:

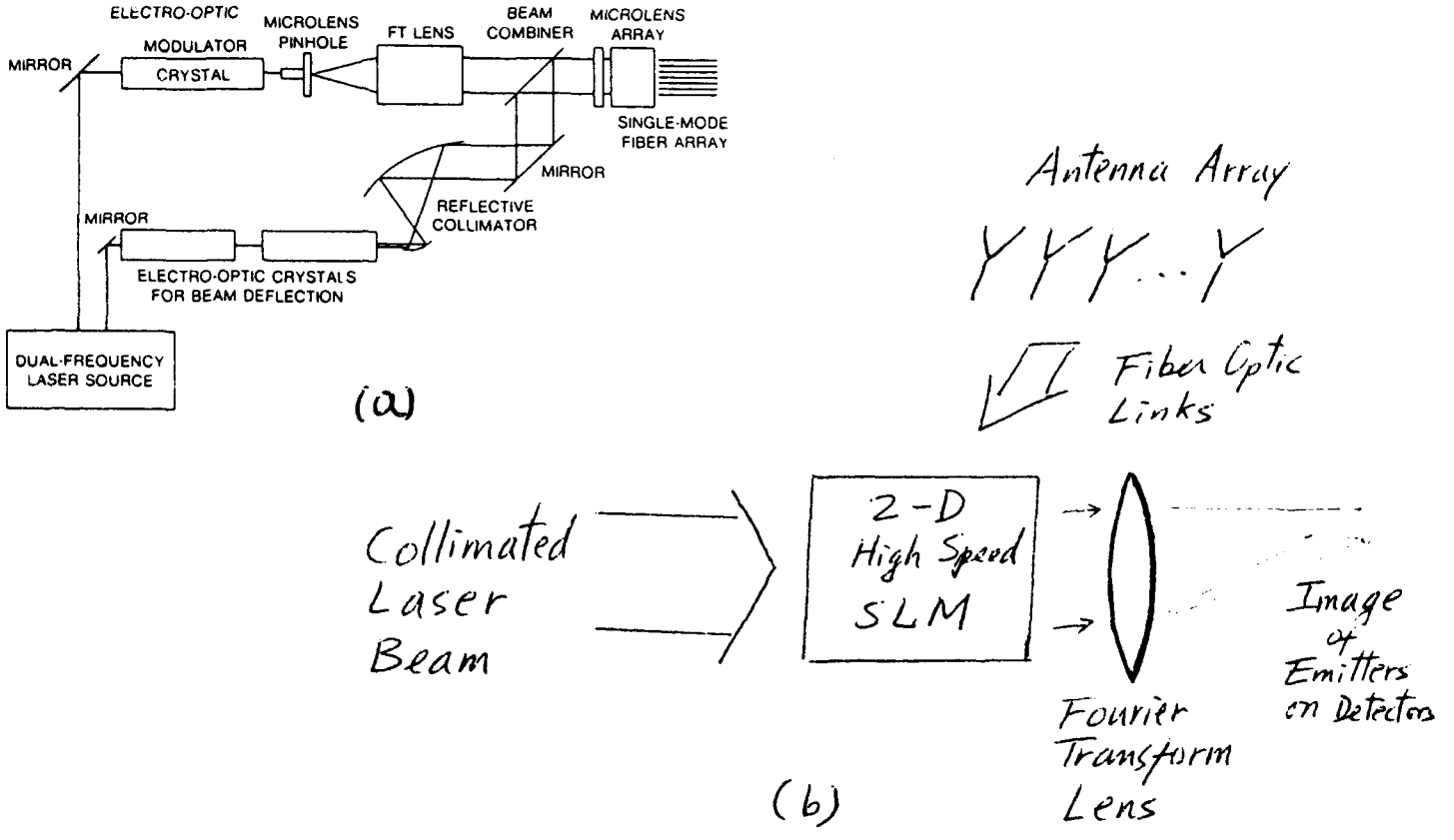

Figure 27, Phased Array Beam Steering Application (a) Transmitter, and (b) Receiver.

Using the acousto-optic imaging 2-D wideband SLM we have an acoustic analogy with the 2-D acoustic transducer array simulating the 2-D microwave array or the 2-D antenna far field. The 2-D microwave field is transfered to optical wavefront by means of the 2-D acoustic field. Optical fourier transform lens can be used to manipulate the modulated optical wavefront to the far field of the acoustic array. Thus, when the acoustic array denotes the far field destination, the required phased array field distribution for achieving such far field pattern is given by the optical output distribution. Figure 27 illustrates such arrangements as applied to (a) generating the array feed signal matrix for one or more signal to be delivered to one or more destinations simultaneously by a phased array, and (b) simultaneous receiving one or more signal from one or more transmitters at different location, (microwave field mapping).

6.1.2 NULL STEERING USING IMAGING ACOUSTO-OPTIC SLM:

A more sophisticated application is for phased array null steering. Null steering is highly powerful for EW, anti-jam and secure communications. A popular algorithms for calculating the weight distribution for adaptive null steering is the Applebaum model. Extensive computation is needed for each weight and the burden of calculating a large array of tap weights in real time is an enormous problem. Using the acousto-optic wideband 2-D SLM, an alternative architecture is proposed for adaptive null steering.

A simplistic view of null steering can be obtained by considering linear superposition of many antenna fields. With a real time imaging receiver, each antenna beam generates an emitter map centered around the antenna beam on the image plane. The image plane of a multi-beam phased array is the overlay of many emitter maps mutually displaced according to the mutual displacement between the antenna beams. The resultant field distribution at an arbitrary location is the vector sum of all the emitters and the sidelobes of emitters falling on that location. To cancel interference due to a given emitter, we can simply generate another emitter map centered around the offending emitter weighted to negate the existing vector sum from the offending emitter. However, the trick is in searching out the offending emitter and its contribution. The proposed new architecture uses correlation on the emitter map while the Applebaum algorithm uses correlation on each antenna elements. Correlation of an array of emitters can be performed optically using multi-channel technologies which may greatly simplify the overall signal processor system.

Figure 28 illustrates a 1-D multi-channel correlator using time integration technique. In this case, all phased array elements shall be rearranged into a linear array of acousto-optic SLM for processing. In a different arrangement shown by figure 29, an imaging acousto-optic 2-D SLM can provide a 2-D array of modulated signal at either the antenna elements or the fourier transform domain of the antenna elements for correlating with a light source signal of given delay and phase. The full array of correlation coefficients for the 2-D array elements can be obtained by systematic tunning the phase of the light source signal. Since correlation of 2-D signal yields a 3-D function, scannning of either the spatial domain or the time domain is needed.

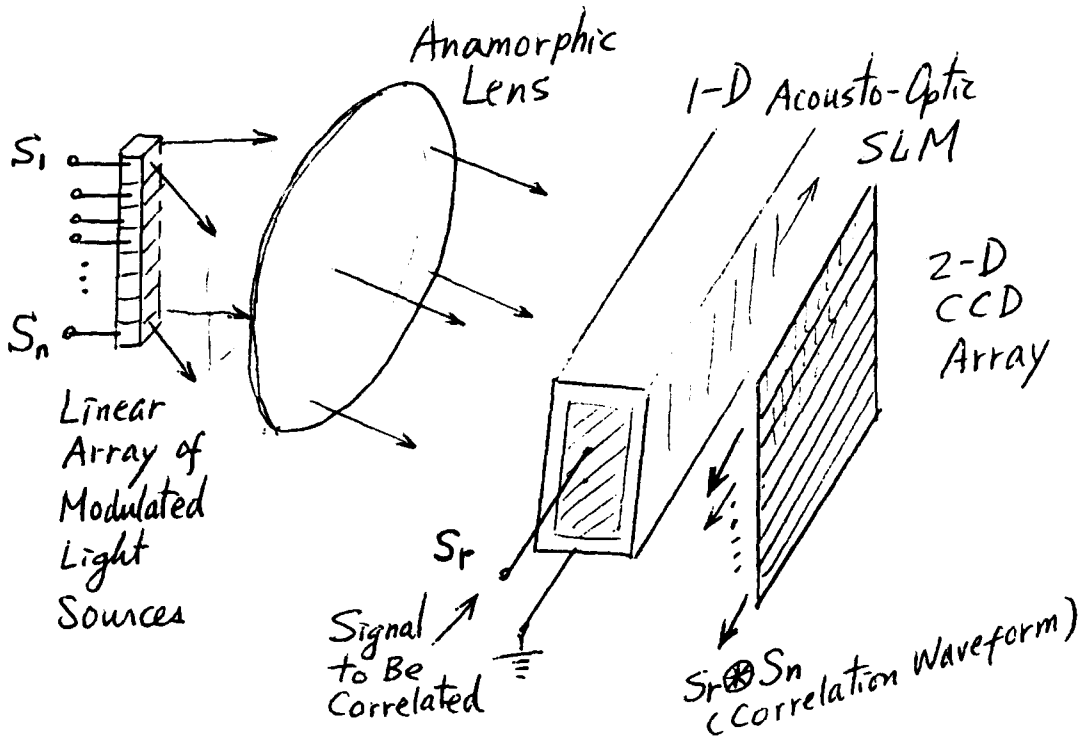

Figure 28, 1-D Multi-Channel Time Integration Correlator for Calculation of Interference Emitter Strength.

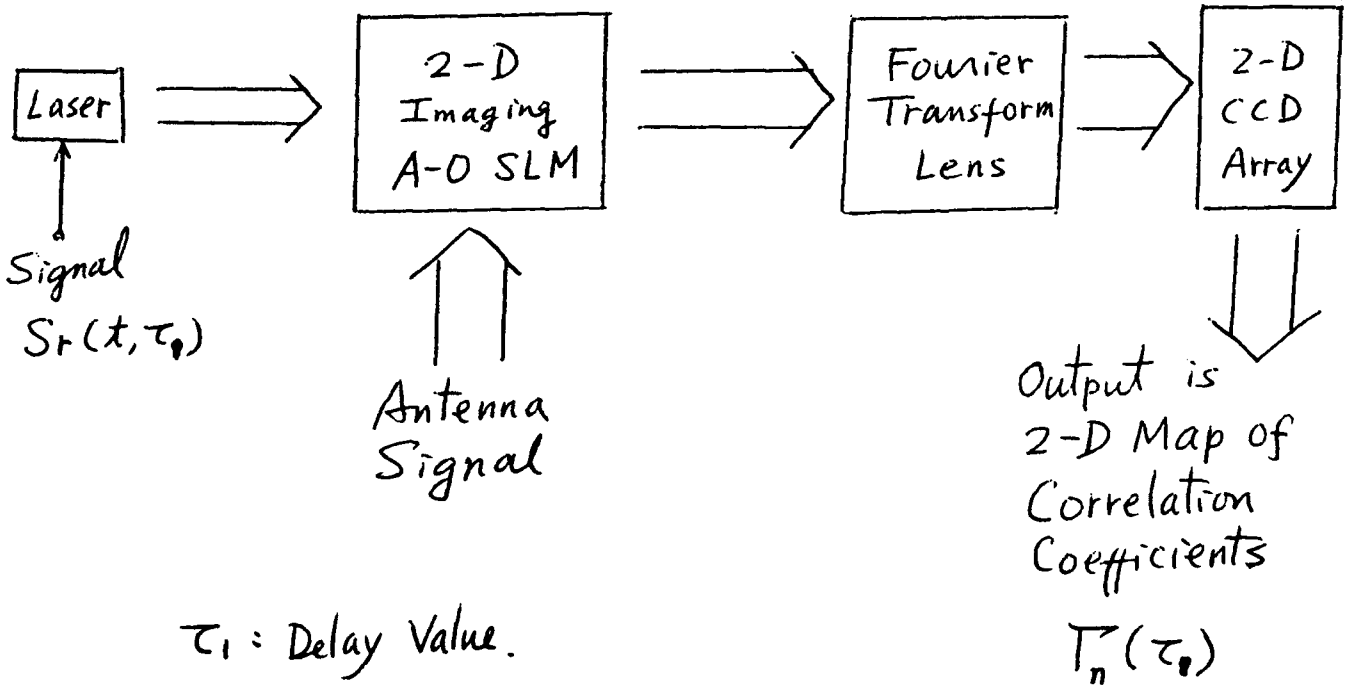

Figure 29, Correlation Coefficient Search for a 2-D array of Elements Using Imaging Acousto-Optic SLM and a Signal Light Source.

6.2 SUMMARY AND RECOMMENDATIONS:

Using an imaging acousto-optic SLM, optical field representing either the antenna elements or the fourier transform of the antenna elements can be generated. The correlation coefficients on the antenna elements are useful for implementing the Applebaum Model. Detail implementation of the Applebaum model processor has been the subject of many recent publications and shall not be described in detail here.

On the other hand, the correlation coefficients on the fourier transform of the antenna elements are measurements of interference strength on the emitter map. As discussed earlier, a negating antenna beam may be directed towards the interfering emitter for adaptive interference cancellation. The generation of the antenna weighs for the negating antenna beam can be calculated using the acousto-optic processor for transmitter signal processing of figure 27(a). The resultant phased array weigh coefficients are the algebraic sum of the beam steering weigh for the main antenna beam and the adaptive interference cancellation weigh for the negating beams.

6.2.1 APPLEBAUM MODEL OR FOURIER TRANSFORM MODEL

The use of multi-channel acosuto-optic correlator can provide interference coefficients either on the antenna elements or on the emitter map (fourier transform domain of the antenna elements). Use of the interference coefficients on the antenna elements and the Applebaum model can lead to effective adaptive cancellation of interfering signal. Use of the interference coefficients on the emitter map and the fourier transform model can also lead to effective cancellation of the interfering signal.

For the case of interference coefficients on the antenna elements, the coefficients are none-zero and are of nearly equal magnitude for all the antenna elements. The measured coefficients are likely to be small equaling to the ratio of signal emitter and interfering emitter. High dynamic range calculations is probably necessary.

For the case of interference coefficients on the emitter map, the coefficients shall be mostly zero with only a few none-zero elements. Furthermore, the strength of the interfering emitter is magnified with the phased array antenna gain at certain emitter map locations. In the mean time, the signal emitter strength at the interfering emitter location is very weak. Thus, the measured interference coefficients is likely to have better signal to noise ratio and dynamic range requiring less demanding processors than needed for the Applebaum model calculations.

In view of the potentially better performances of the adaptive cancellation processor using the fourier transform model, further analytical study of the fourier transform adaptive processor is recommended.

7.0 PROGRAM SUMMARY AND RECOMMENDATIONS:

This phase I SBIR program covers broad areas from two advanced device concepts to sophisticated system architectures. Both experimental and analytical investigations have been conducted to evaluate the feasibility for advanced optical processors for phased array antenna applications. Despite of limited resources for such diverse investigations, we have successfully demonstrated the feasibility and explored the technical issues of these new device and system concepts. The results are positive. The results and recommendations will be described as follows.

7.1 SUMMARY OF PHASE I PROGRAM RESULTS:

During the phase I SBIR program, we have successfully conducted experimental demonstration of (1) the use of photo-refractive self-pumped-phase-conjugation mirror for detecting phase drifts in a polarization maintaining single mode optical fiber, and (2) the operation principle of an imaging acousto-optic spatial light modulator array. The physical properties of the photo-refractive SPPC material, KNSBN, and of a KITTY SPPC mirror device arrangement for weak signal has been measured. Relatively fast KITTY SPPC mirror response time with a weak signal beam (substantially under 1 mw) after long propagation delay (10 meters) has been successfully demonstrated. Fast rise time in the order of nano-seconds has been measured using two make-shift acousto-optic devices in imaging acousto-optic diffraction mode of operation. The spatial resolution capability of imaging acousto-optic SLM has also been demonstrated experimentally.

We have also conducted basic analysis on the operation of the imaging acousto-optic spatial light modulator array. The resolution-frame rate product of such devices is superior to that of a conventional acousto-optic spatial light modulator. More importantly, the imaging acousto-optic SLM is more suited for high speed and 2-D operations than the conventional acousto-optic SLM devices.

The use of multi-channel optical correlators for measurement of interference coefficients in a phased array antenna has been investigated. Using an imaging acousto-optic SLM array, the intereference coefficients can be measured either at the antenna elements or at the fourier transform domain of the antenna elements. Use of the interference coefficients at the antenna elements and the Applebaum model for adaptive noise cancellation is well known and is subject of intensive investigations recently. Use of the interference coefficients at the fourier domain of the antenna elements generates an interference emitter map. Due to the phased array antenna gain, measurements of interference coefiicients at the fourier transform domain is deemed easier and more accurate. Since only a few of the interference coefficients at the fourier transform domain will be none-zero, handling of the coefficients shall be also easier.

An additional advantage of the fourier transform domain processing is the many other usefulness of the interference emitter map. Its physical meaning allows the use for sophisticated communications, EW and ESM applications.

7.2 ISSUES FOR IMPLEMENTATION OF THE ADVANCED TECHNIQUES:

The technical issues for implementation of the jitter free fiber optic RF distribution system, the imaging acousto-optic sptial light modulator, and the fourier domain phased array adaptive cancellation processor are given as follows.

A. For Jitter Free RF Distribtuion:

(1) Development of a high power (200mw to 1 watt) signle longitudinal mode, single transverse mode stabilized injection laser diode.

(2) Development of a fast KITTY SPPC Mirror operating in the near IR ILD wavelengths.

(3) Development of the guidedwave optical phase modulator module for the detection and compensation of phase drifts through optical fibers.

(4) Demonstration of a jitter free RF distribution link using photo-refractive technology.

B. For Development of A Fast Frame Rate Acousto-Optic SLM:

(1) Design and construction of an imaging acousto-optic spatial light modulator array with greater than 32 by 32 elements.

(2) Detail evaluation of the resolution, modulation, frame rate, and far field optical quality of an imaging acousto-optic spatial light modulator array with greater than 32 by 32 elements.

(3) Development of novel data interface techniques other than direct electrical connections for addressing the transducer array of the imaging acousto-optic SLM.

C. For A Fourier Domain Phased Array Adaptive Cancellation Processor:

(1) Detailed mathematical analysis and modeling of the fourier transform adaptive cancellation processor for comaprison with the Applebaum model.

(2) Software simulation of the fourier domain phased array adaptive cancellation processor.

(3) Experimental evaluation of fourier transform beam forming processor performances as transmitter and as receiver.

(4) Demonstration of using an imaging acousto-optic SLM to provide interference coefficients measurements on the antenna elements and on the fourier domain of antenna elements.

7.3 RECOMMENDED TASKS FOR FOLLOW ON PHASE II PROGRAM:

Based on the phase I program findings, a phase II program for further investigation of the propsed new devices and architectures appear worthwhile. However, the rather

diverse research areas covered under this program may present a problem even with the resources of a phase II program. Thus, the recommended phase II research shall be limited to selected areas only.

Among the three major areas of interest, the jitter free RF distribution system can be singled out as an area of highest payoff potential. Success of the distribution system alone can result in enhenced fiber-optic microwave phased array antenna performances and many other usefull applications. On the other hand, the new adaptive processor architecture and the imaging acousto-optic SLM may need more developments and may be a little more limited in applications. Therefore, the phase II recommendations is focused on the development of a jitter free fiber optic RF distribution link.

The recommended developmental tasks for the phase II program are

TASK 1) Development of a high power (200mw to 1 watt) signle longitudinal mode, single transverse mode stabilized injection laser diode.

TASK 2) Development of a fast KITTY SPPC Mirror operating in the near IR ILD wavelengths.

TASK 3) Development of the guidedwave optical phase modulator module for the detection and compensation of phase drifts through optical fibers.

TASK 4) Demonstration and evaluation of a jitter free RF distribution link using photo-refractive technology.

8.0. REFERENCES:

1, M. de La Chapelle and H.P. Hsu, "Characterization of Fiber Optic Links for Microwave Signal Transmission," SPIE Proc. 789, p. 32, 1987.

2, D.L. Baldwin et.al., "Laser Link Performance Improvement with Wideband Microwave Impedance Matching," SPIE PROC. 1476, p. 46, 1991.

3, D.J. Fitzmartin et. al., "Coherent optical Modulation for Antenna Remoting," SPIE PROC. 1476, p. 56, 1991.

4, D.dolfi, J-P Huignard, and M. Baril,"Optically Controlled True Time Delays for Phased Array Antenna," SPIE PROC. 1102, p. 152, 1989.

5, G.A. Koepf, "Optical Processor for Phased Array Antenna Beam Formation", SPIE Proc. Vol. 477, p. 75, 1984.

6, W. Birkmayer, C. Shaffer, B. Hosselbarth,"Scenarios and System Architectures Advantageous for Optical Technologies in Phased Array Antennas," SPIE Proc.1217, p. 14, 1990.

7, I.L. Newberg, A.A. Walston, J.J. Lee, and W.W. Ng, G.L. Tangonan, "Electro-Optical Switch for Antenna Beamsteering," SPIE Proc. 1217, p. 126, 1990.

8, W.A. Penn, R. Wasiewicz, and R. M. Iodice,"Optical Adaptive Multipath Canceller for Surveillance Radar," SPIE Proc. 1217, p. 151, 1990.

9, C. DeCusatis and P. Das,"Optical Controller for Adaptive Phased Array Antennas Using Neural Network Architecture", SPIE Proc. 1217, p. 161, 1990.

10, J. G. Von Saders and V.H. Syed,"An Optical Adaptive Processor for Null Steering in Phased Array Antennas," SPIE Proc. 789, p. 80, 1987.

11, M. H. Berry and D. M. Gookin," Null Steering with Fixed Delays", SPIE Proc. 1217, p. 262, 1990.

12, N.V. Jesperson and P. R. Herczfeld,"Comparison of Fiber Optic and Space Feed for Large Aperture Phased Array Antennas," SPIE Proc. 789, p.88, 1987.

13, R.M. Montgomery, "Acousto-Optic/Photorefractive Processor for Adaptive Antenna Arrays", SPIE. Proc. 1217, p. 207, 1990.

14, D. Psaltis and J. Hong, "Adaptive Acousto-Optic Filter," Applied Optics, V. 23, No. 19, p. 3475, Oct.1, 1984.

15, W.A. Penn,et.al,"Acousto-Optic Adaptive Processing(AOAP)",RADC-TR-83-156,Dec.'83. and W.A. Penn, "Acousto-Optic Adaptive Processing (AOAP) - Phase II", RADC-TR-86-188, Nov. 1986.

16, Bob Berinato, "Acousto-Optic Signal Processor for Adaptive Filtering" SPIE Proc. Vol. 1296, p. 232, 1990.

17, J.F. Rhodes,"Adaptive Filter with a Time-Domain Implementation Using Correlation Cancellation Loops," Applied Optics, V.22, No. 2, p. 282, Jan 15, 1983.

18, A. Vanderlugt,"Adaptive Optical Processor",Appl.Opt. 21,No.22, p.4005,Nov.15,1982.

19, D.M. Pepper, "Nonlinear Optical Phase Conjugation," Optical Engineering 21, p. 156, 1982.

20, A. Yariv and P. Yeh, "Optical Waves in Crystals," John Wiley and Son, 1984.

21, A.E. Chiou, T.Y. Chang, and M. Khoshnevisan, "Characterization of a Photorefractive Phase Conjugator with Large Dynamic Range and Wide Field of View," Rockwell International, Science Center, To Be Published.

22, H.C. Chen, D.L. Sun, and Q.Z. Jiang, "Growth ans Properties of A New Type Photorefractive Crystal," 1992 Crystal Growth Conference, San Diego, Aug. 17-21, 1992.

23, R. Montgomery and M. Lange, "Photorefractive Adaptive Filter Structure with 40 dB Interference Rejection," Applied Optics, 30, 2844-2849, 1991.

24, M.G. Cohen and E.I. Gordon, "Acoustic Beam Probing Using Optical Techniques," BSTJ., Vol. XLIV, p. 693, April 1965.

25, E.I. Gordon, "A Review of Acousto-Optical Deflection and Modulation Devices," Proc. IEEE, Vol. 54, 10, p.1391, 1966.

26, J.W. Goodman, "Introduction to Fourier Optics," McGraw Hill, 1968.

27, A. Korpel, "Visualization of the Cross-Section of a Sound Beam by Bragg Diffraction of Light," Appl. Physics Lett., 9, p. 425, 1966.

28, A. Korpel, "Acoustic Imaging by Diffracted Light - Two Dimensional Interaction," on the book of "Acoustic Holography I, chapter 10", and on IEEE Transactions on Sonic and Ultrasonics, Vol. SU-15, No. 3, July 1968.

29, R.W. Damon, W.T. Maloney, and D.H. McMahon, "Physical Acoustics, Vol VII, Chapter 5, Interaction of Light with Ultrasound," Editor: Mason, Academic Press.

30, E.H. Young and S.K. Yao," Design Considerations for Acousto-Optic Devices," Invited Paper, Proc. IEEE, vol. 69, p. 54, 1981.

31, E.H. Young andS.K. Yao, "Linear Array Acousto-Optic Devices," Proc. IEEE Ultrasonics Symposium, Annapolis, Md., p. 666, 1976.

32, S. Haykin, Adaptive Filter Theory, Prentice Hall, Englewood Cliffs, New Jersey, 1986.

33, R.T. Compton, Jr.,Adaptive Antennas, Prentice Hall,Englewood Cliffs, N.J., 1988.

34, P. Kellman, " Time Integrating Optical Signal Processing," Acousto-Optic Bulk Wave

Devices, J. Houston, Ed., Proc. SPIE, Vol. 214, p. 63, 1979.

35, T.R. Bader, " Acopusto-Optic Spectrum Analysis: A High Performance Hybrid Technique," Applied Optics, Vol. 18, p. 1668, 1979.

36, P.S. Guifoyle, D.L. Hecht, and D.L. Steinmetz, " Joint Transform Time Integrating acousto-Optic Correlator for Chirp SPectrum Analysis," Active Optic Devices, Proc. SPIE, Vol. 202, p. 154, 1979.

37, William T. Rhodes, "Acousto-Optic SIgnal Processing: Convolution and Correlation," Proc. IEEE, vol. 69, p. 65, 1981.

38, Terry M. Turpin, " Spectrum Analysis Using Optical Processing," Proc. IEEE, Vol. 69, p. 79, 1981.